Article

Mineralogy and Geochemistry of Late Permian Coals within the Tongzi Coalfield in Guizhou Province, Southwest China

Baoqing Li [1],*, Xinguo Zhuang [1], Xavier Querol [1,2], Natalia Moreno [2] , Linjian Yang [3], Yunfei Shangguan [1] and Jing Li [1]

[1] Key Laboratory of Tectonics and Petroleum Resources (China University of Geosciences), Ministry of Education, Wuhan 430074, China; xgzhuang@cug.edu.cn (X.Z.); xavier.querol@idaea.csic.es (X.Q.); SGyunfei@cug.edu.cn (Y.S.); lijing02003140@163.com (J.L.)

[2] Institute of Environmental Assessment and Water Research, CSIC, C/Jordi Girona 18–26, 08034 Barcelona, Spain; natalia.moreno@idaea.csic.es

[3] No. 106 Geological Team of Guizhou Province Geology and Mineral Bureau, Zunyi 563000, China; wanw535@126.com

* Correspondence: bqli1986@126.com or libq@cug.edu.cn

check for updates

Abstract: The lowermost Late Permian coal seam (C4 Coal) in the Tongzi Coalfield offers an opportunity to investigate the influence of terrigenous detrital materials from the Qianbei Upland on the mineralogical and geochemical patterns of the C4 Coal. The minerals are mainly dominated by pyrite and, to a lesser extent, tobelite, kaolinite, and calcite, along with traces of Al-oxyhydroxide minerals. The various degrees of marine influence may have resulted in the variation in the amount of Fe-sulfides (e.g., pyrite) and elements having Fe-sulfides affinity. Furthermore, the abundant Fe ions involved in the formation of Fe-sulfides were most likely derived from the claystone on the Qianbei Upland. The tobelite identified in the C4 Coal probably originated from the interaction between pre-existing kaolinite and NH_4^+ from NH_3 released from the thermally affected organic matter at least shortly after the highly volatile bituminous stage under NH_4^+-rich and K^+-poor conditions. The terrigenous detrital materials were derived from two possible sediment-region sources—the Qianbei Upland and Kangdian Upland—which is different from Late Permian coals in Western Guizhou Province. The claystone on the Qianbei Upland may have served as parent rock, as indicated by the presence of the Al-oxyhydroxide minerals as well as low SiO_2/Al_2O_3 ratio (0.66 on average) and low quartz content. Meanwhile, the detrital materials from the Kangdian Upland most likely originated from the erosion of the felsic rocks at the uppermost part of the Kangdian Upland, as evidenced by the high Al_2O_3/TiO_2 ratio (36.0 on average) and the strongly negative Eu anomaly (0.61 on average).

Keywords: Late Permian coal; tobelite; Kangdian Upland; Wujiaping Formation; Guizhou Province

1. Introduction

Knowledge of mineralogy and geochemistry of coals is of great importance, not only in guiding coal utilization, but also in deducing coal-forming environment, sediment-area source, volcanic activity, hydrothermal fluid activity, and regional geological setting [1–5].

It has commonly been assumed that the Kangdian Upland is the predominant sediment-source area for the Late Permian coal-bearing strata in Southwestern China, especially in Chongqing, Yunnan, Sichuan, and Western Guizhou Provinces [5–7]. The Kangdian Upland consists essentially of the Emeishan basalts, along with traces of the felsic rocks occurring at the uppermost part of the Kangdian Upland [8–10], the former of which are almost entirely the parent rocks for inorganic constituents in

the Late Permian coals in Southwestern China [1,5,11–19]. Recent studies, however, have suggested that the Emeishan felsic rocks at the uppermost part of the Kangdian Upland may have supplied detrital materials into the lowermost Late Permian coals and associated non-coal rocks in Sichuan Province, Chongqing city, and Western Guizhou Province, Southwest China [20–25]. However, it is not clear if these felsic rocks may have been the parent rocks for the Late Permian coals in Eastern Guizhou Province, Southwest China. Aside from the Kangdian Upland, some subordinate uplifted regions, such as the Qianbei Upland and/or Wenshui Highland (Figure 1), may have contributed detrital materials into the coal-forming environments [6,20,22]. For example, China Coal Geology Bureau [6] and Dai et al. [20,22] indicated that the Wenshui Highland may serve as the subordinate sediment source region and supplied trace amounts of mafic terrigenous materials to the Late Permian coals in Chongqing City, Southwest China.

The mineralogical and geochemical patterns of Late Permian coals in western Guizhou Province have been extensively investigated [11–18], but those in northeastern Guizhou Province are not known. The Tongzi Coalfield is distributed in the northeastern Guizhou Province and is adjacent to the Qianbei Upland (Figure 1), which may provide an opportunity to estimate the effect of materials influx from the Qianbei Upland on mineralogical and geochemical patterns. In this study, we report and interpret mineralogical and geochemical data on the C4 Coal at the lowermost part of Late Permian coal-bearing strata in the Tongzi Coalfield, mainly to address if the Emeishan felsic rocks and the Qianbei Upland influenced the mineralogical and geochemical patterns of the C4 Coal, and to discuss the origin of minerals identified in the coals.

2. Geological Setting

2.1. Coal-Bearing Strata

Guizhou Province, located in Southwestern China (Figure 1A), contains abundant coal resources. The Tongzi Coalfield is situated in the Northeastern Guizhou Province (Figure 1B). The Permian strata in the Tongzi Coalfield may be divided, in ascending order, into the Early Permian Liangshan Formation, Middle Permian Qixia, and Maokou Formations, as well as Late Permian Wujiaping and Changxing Formations. Among these, the Late Permian Wujiaping Formation is the dominant coal-bearing sequence [6,7].

The Middle Permian Maokou Formation is extensively distributed in Southwestern China and consists mainly of marine limestones [7,26]. At the end of the Middle Permian, the Maokou Formation experienced extensive weathering and erosion due to the Emeishan plume-induced crust uplift in Southwestern China that is known as the Dongwu Movement by the Chinese geological community [27], leading to the formation of erosional unconformity and karstic surfaces on the top of the Maokou Formation limestones [26,28]. Subsequently, the Emeishan volcanic eruption occurred and volcanic ash fell on to the karstic surface [6,21]. The erupted Emeishan volcanic rocks experienced weathering and leaching, forming weathering remnants at the top of the Maokou Formation [6,21]. The weathering remnants were transported into the karstic surfaces to form the paleo-weathering crust at the top of the Maokou Formation in the Eastern Guizhou Province [29]. The paleo-weathering crust was subsequently overlaid by marine sediments of the Late Permian Wujiaping Formation due to marine transgression [7].

The Late Permian Wujiaping Formation, a primarily coal-bearing stratum in the Tongzi Coalfield, unconformably overlies the Middle Permian Maokou Formation and conformably underlies the Late Permian Changxing Formation (Figure 2). The Wujiaping Formation is subdivided into three separate intervals in terms of lithological composition and coal-bearing characteristics (Figure 2). The lowermost interval (I) of the Wujiaping Formation is made up of a claystone layer with a thickness of 1.3–3.4 m that unconformably overlies the Maokou Formation limestone and directly underlies the C4 Coal (Figure 2); the claystone contains abundant pyrite nodules and bands. The second interval (II) has an approximate thickness of 21 m and was the result of sedimentary deposition in a lagoon-tidal flat

environment [7,30]. It consists mainly of flint nodule-bearing limestones, mudstones, and one to four coal seams. The C4 Coal, located at the bottom of this interval, is a major workable coal bed and is transgressively overlaid by marine limestone (Figure 2). The C3 coal is an unworkable coal bed and its thickness ranges from 0.15 to 0.49 m, with an average of 0.35 m. The third interval (III), with a thickness of approximately 50 m, is composed mainly of limestones intercalated with thin layers of mudstones and siltstones (Figure 2) and formed in a marine carbonate platform environment [7].

The Changxing Formation, overlying the Wujiaping Formation, is about 55 m thick and does not contain coal seams. The Changxing Formation consists almost entirely of marine limestones intercalated with thin layers of mudstones and also formed in a carbonate platform environment.
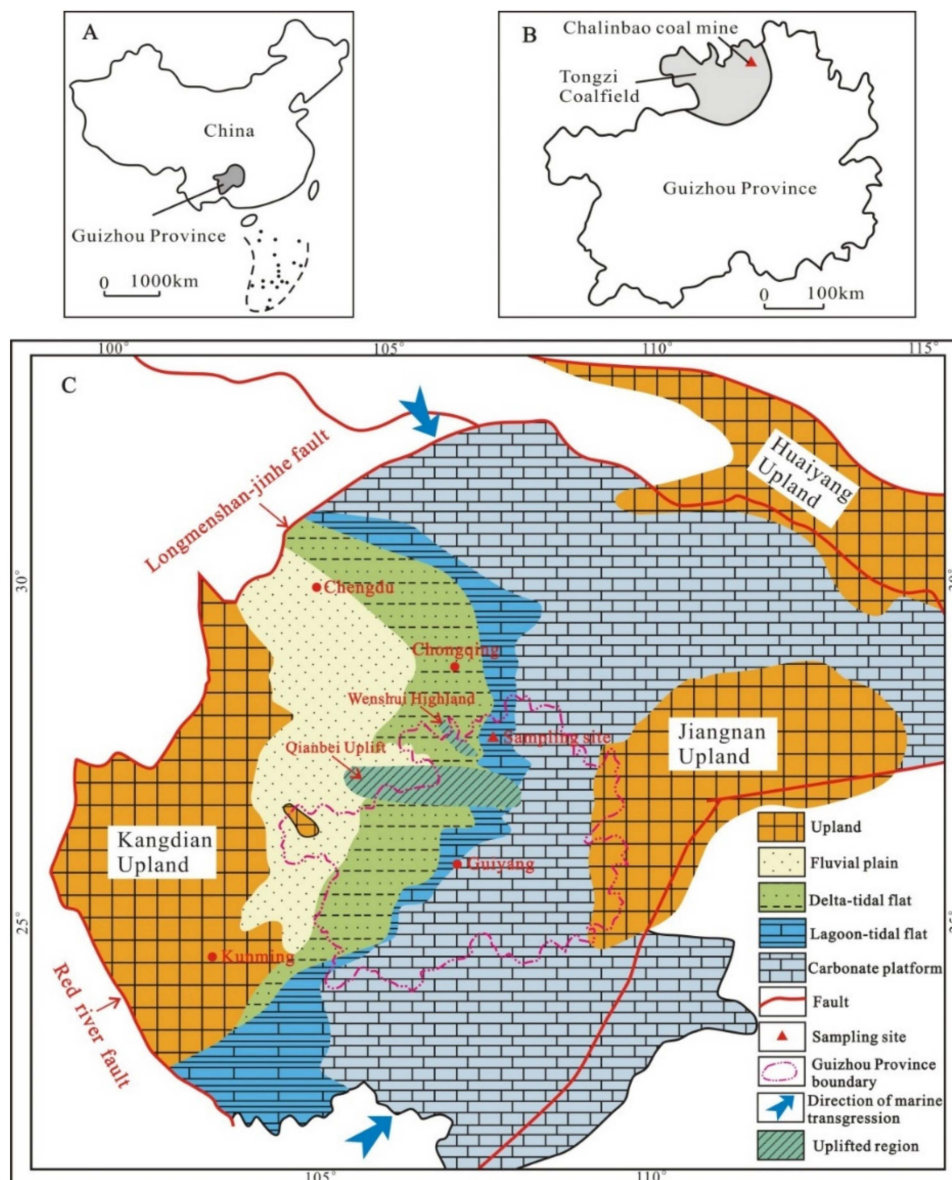
Figure 1. Maps of the study area: (**A**): Map of China showing the location of Guizhou Province, southwestern China. (**B**): Location of the Tongzi Coalfield. (**C**): Palaeogeography of early Late Permian period modified from [6,7,30].
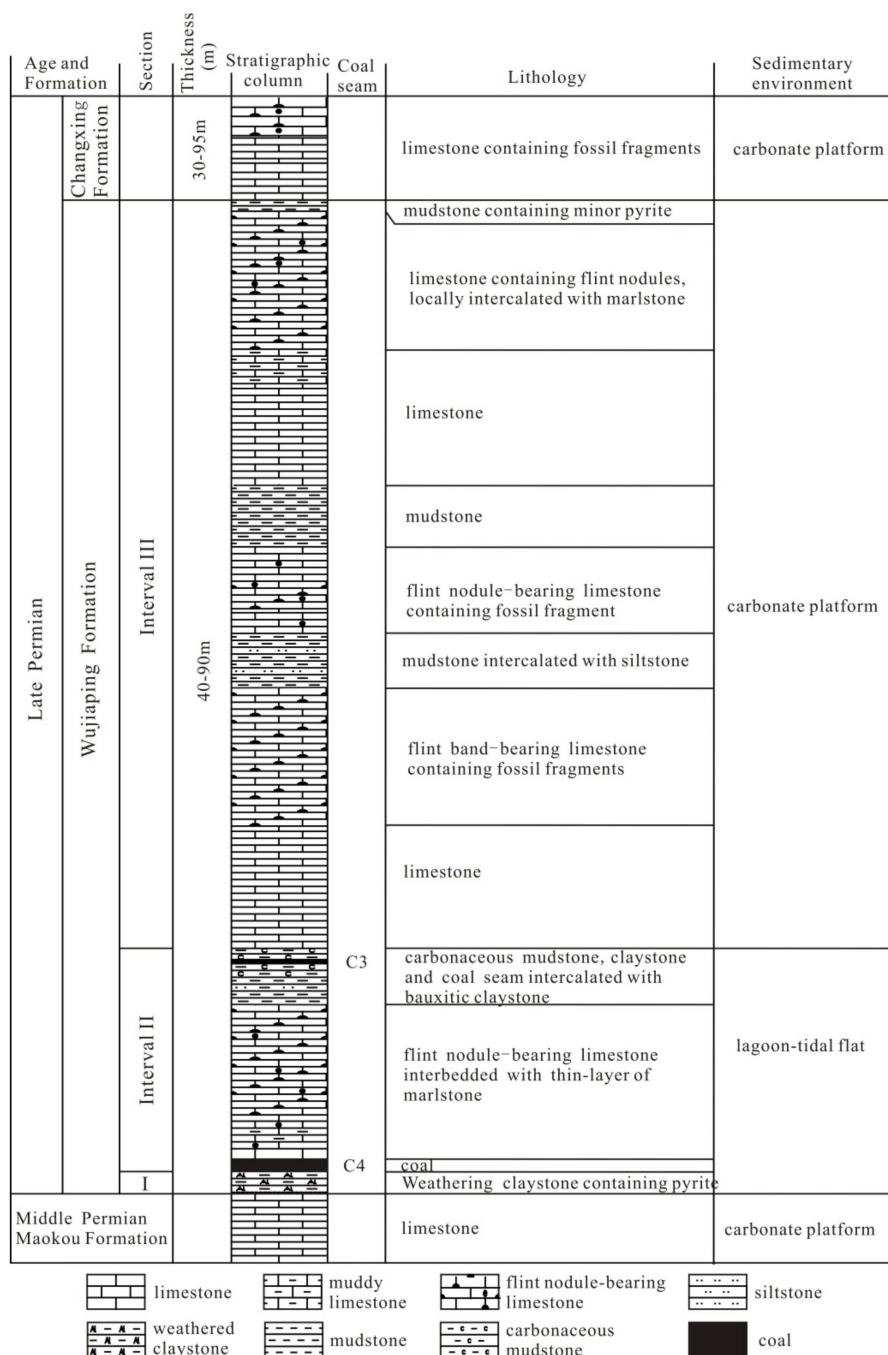
Figure 2. Sedimentary sequence of the Late Permian Wujiaping Formation in the Tongzi Coalfield (Based on the exploration data from Guizhou Province Geology and Mineral Bureau).

2.2. Sediment-Source Region

As stated above, the Kangdian Upland, situated to the West of Guizhou Province (Figure 1C), is generally considered as being a predominant mineral matter source for the Late Permian coal-bearing strata in Guizhou Province [5–7]. It is composed mainly of the Emeishan low-Ti and high-Ti basalts and, to a lesser extent, picrites and pyroclastic rocks, along with trachytes and rhyolites, as well as felsic and mafic-ultramafic intrusions occurring at the uppermost part of the Kangdian Upland [9,10,31–36]. The Qianbei Uplift and/or Wenshui Highland to the South of the sampling site (Figure 1C) may also serve as sediment-source regions for the lower part of the Wujiaping Formation (Figure 2) but was inundated

when the upper part of the Wujiaping Formation was being deposited due to a more extensive marine transgression [6,30].

3. Methodology

A total of sixteen bench samples were collected from the underground working face of Chalinbao coal mine in the Tongzi Coalfield (Figure 1B). Each coal bench sample was cut from an area about 10 cm wide and 10 cm deep and the collected samples, including fourteen coal bench samples and two floor samples, are shown in Figure 3. Samples collected were instantly kept in sealed plastic bags to minimize contamination and oxidation.
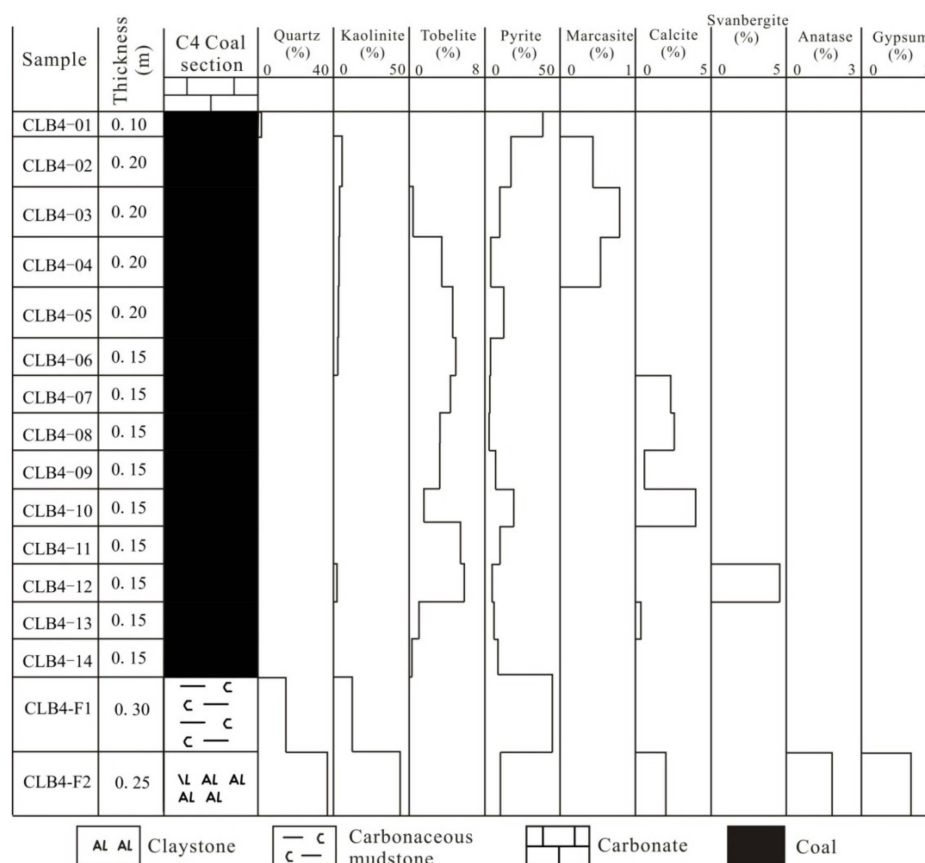

Figure 3. Vertical distribution of the minerals identified in the C4 Coal (on whole-coal basis).

The samples were crushed and milled to pass 200 mesh (75 μm) for proximate, ultimate, mineralogical, and geochemical analysis. The bulk samples were prepared and polished for the SEM-EDS analysis. Proximate analysis (moisture content, ash yield, volatile matter yield) was performed according to ASTM Standards D3173-11 [37], D3174-11 [38], and D3175-11 [39]. Ultimate analysis (C, H, S, N) was carried out using a Vario EL III Elemental Analyzer (Vario EL III, Elementar Trading (shanghai), Shanghai, China). Mean random reflectance of vitrinite (Ro) was carried out using a Leica DM-4500P microscope (Leica, Elementar Trading (shanghai), Shanghai, China). Two field emission-scanning electron microscopes SEM-EDS (FEI Quanta™ 450 FEG, Thermo Fisher Scientific, Waltham, MA, USA; ZEISS EVO LS 15, Carl Zeiss AG, Jena, Germany) were used to identify the modes of mineral occurrences and element distribution within minerals.

Sample preparation and analytical procedure for mineralogical identification were described in more detail by Li et al. [40]. Mineralogical compositions were determined by powder X-Ray Diffraction (XRD) using a Bruker D8 A25 Advance, θ-θ diffractometer with CuKα1 radiation, Bragg-Brentano geometry, and a position sensitive LynxEyeXE detector (Bruker D8 A25 Advance, Leipzig, Germany).

The diffractogram was obtained at 40 kV and 40 mA, scanning from 4° to 60° 2θ with a step size of 0.019° and a counting time of 0.1 s/step maintaining the sample in rotation (15/min) during the analysis. Semi-quantitative XRD analysis was performed by using the Internal Reference Method devised by Chung [41].

For geochemical analysis, the above milled and sieved materials were acid-digested following a two-step digestion method as previously reported by Querol et al. [42]. The solution was then assayed for major elements using Inductively Coupled Plasma Atomic-Emission Spectrometry (ICP-AES, Iris Advantage TJA Solutions, Thermo Fisher Scientific, Waltham, MA, USA) and for trace elements using Inductively Coupled Plasma Mass Spectrometry (ICP-MS, X-Series II Thermo, Thermo Fisher Scientific, Waltham, MA, USA). Molybdenum Blue Spectrophotometry was used to determine Si content according to GB/T 1574-2007 [43]. Blank samples and international reference material (SARM-19) were also performed following the same procedure to test the precision of the digestion and the analytical method. The analytical precision was better than ±20.0% for K, Mg, P, Be, B, Sc, Cu, Zn, Se, Sr, and Sn, and better than ±10.0% for Zr, Nb, Mo, Tb, Hf, Ta, and better than ±5.0% for other elements.

Ion exchange tests carried out in this study to support the occurrence of tobelite (detected by XRD analysis). To this end, a NaCl solution was used to suspend specific powdered coal samples to induce the Na^+–NH_4^+ exchange in tobelite-bearing coals. One litre of NaCl saturated solution was prepared by dissolving NaCl reagent with distilled Milli-Q water. The ion exchange tests were carried out by mixing 25 and 50 mL of NaCl solution respectively with 0.5 g of selected powdered coal samples (CLB4-2 and CLB4-5+6, a mixture of CLB4-5 and CLB4-6) in screw cap bottles, which were placed to a Heidolph REAX 2 Shaker (Heidolph, Schwabach, Germany) with continuous stirring at room temperature for 24 h. After stirring, these suspensions were filtered through Whatman filter paper, and the NH_4^+ contents in filtrates were immediately determined by ion selective electrode (ISE).

4. Results

4.1. Coal Chemistry and Coal Rank

The results of the proximate and ultimate analyses, as well as vitrinite reflectance of the studied samples, are summarized in Table 1. The moisture content in the C4 Coal from the Chalinbao underground coal mine ranges from 0.7% to 1.8%, indicating a special-low moisture content (<6.0% for special-low moisture; MT/T 850-2000 [44]). The ash yields vary between 7.4% and 40.6%, with an average of 15.7%, but mostly <20% ash yield, indicating mostly super-low to low-ash coals following Chinese Standards GB/T 15224.1-2010 [45] (0%–10% for super-low ash coal and 10%–20% for low-ash coal). The volatile matter yields range from 12.8% to 26.7%, with an average of 15.3%, but mostly between 12.8% and 18.2%, indicating a low volatile bituminous coal rank according to ASTM D388-12 [46] (14%–22% for low-volatile bituminous). The vitrinite random reflectance (Ro) values ranging from 1.59% to 1.95% (1.76% on average) also indicate a low-volatile bituminous rank. The Ro value shows no correlation with the volatile matter yield in all coal benches but correlates negatively to the volatile yield (r = −0.88; Figure 4A) in the coals with <18.0% ash yield. This possible explanation is that a more proportion of volatile matter in the coals with >18.0% ash yield may have originated from the mineral phases (e.g., pyrite), as attested by the significant correlation of volatile matter yield-pyrite (r = 0.96; Figure 4B). The sulfur contents vary between 2.3% and 24.1%, with an average of 7.0%, indicating medium to high-sulfur coals (1%–3% for medium-sulfur coal, >3% for high-sulfur coal [47]). The upper and lower portions of the C4 Coal are dominated by high-sulfur coals, while the middle part consists mostly of medium-sulfur coals (Figure 5). The floor samples also have high sulfur contents (Figure 5).

Table 1. Thickness (m), proximate and ultimate analyses (wt. %), and vitrinite random reflectance (%) of the coal and floor samples from the Chalinbao underground coal mine in the Tongzi Coalfield.

Sample	Thickness	M_{ad}	A_d	VM_{daf}	C_{daf}	H_{daf}	N_{daf}	$S_{t,d}$	R_o
CLB4-1	0.10	1.51	40.6	26.7	70.0	4.13	0.64	24.1	1.81
CLB4-2	0.20	1.80	22.2	18.0	71.9	4.23	0.90	13.2	1.75
CLB4-3	0.20	1.35	14.1	14.2	83.2	4.53	1.08	4.9	1.74
CLB4-4	0.20	1.30	10.7	12.8	87.9	4.73	1.25	2.6	1.95
CLB4-5	0.20	1.17	19.6	14.8	81.5	4.76	1.24	5.7	1.73
CLB4-6	0.15	0.74	10.9	13.8	87.0	4.59	1.28	2.7	1.87
CLB4-7	0.15	0.91	9.8	12.9	87.8	4.65	1.33	2.3	1.89
CLB4-8	0.15	1.18	8.2	12.8	87.9	4.82	1.33	2.7	1.90
CLB4-9	0.15	1.43	10.8	13.3	86.4	4.67	1.31	4.8	1.75
CLB4-10	0.15	1.16	24.4	18.2	74.1	3.76	0.99	14.2	1.70
CLB4-11	0.15	1.43	15.3	13.0	84.7	4.74	1.54	6.1	1.63
CLB4-12	0.15	1.35	16.9	14.7	86.3	4.80	1.51	3.3	1.67
CLB4-13	0.15	1.57	7.4	15.0	87.0	4.88	1.29	4.7	1.62
CLB4-14	0.15	1.56	8.9	14.7	85.0	4.46	1.16	6.5	1.59
CLB-F1	0.30	nd	72.7	nd	nd	nd	nd	24.4	nd
CLB-F2	0.25	nd	100.0	nd	nd	nd	nd	5.1	nd

M, moisture; A, ash yield; VM, volatile matter yield; C, carbon; H, hydrogen; N, nitrogen; St, total sulfur; ad, air-dry basis; d, dry basis; daf, dry and ash-free basis; Ro, vitrinite random reflectance; nd, not detected.
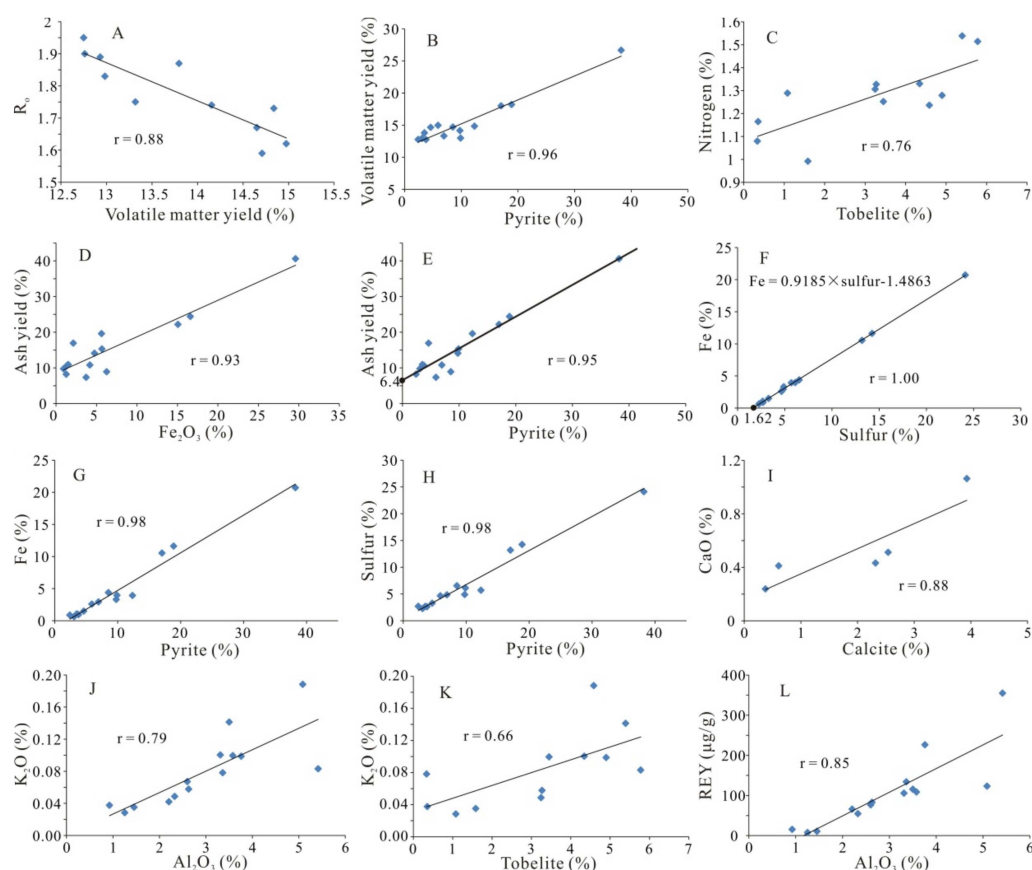
Figure 4. Correlation coefficient of selected elements, minerals, volatile matter yield, ash yield, and Ro. Correlation of Ro-volatile matter yield (**A**), pyrite-volatile matter yield (**B**), tobelite-nitrogen (**C**), Fe_2O_3-ash yield (**D**), pyrite-ash yield (**E**), sulfur-Fe (**F**), pyrite-Fe(**G**), pyrite-sulfur (**H**), calcite-CaO (**I**), Al_2O_3-K_2O (**J**), tobelite-K_2O (**K**), and Al_2O_3-REY (**L**).
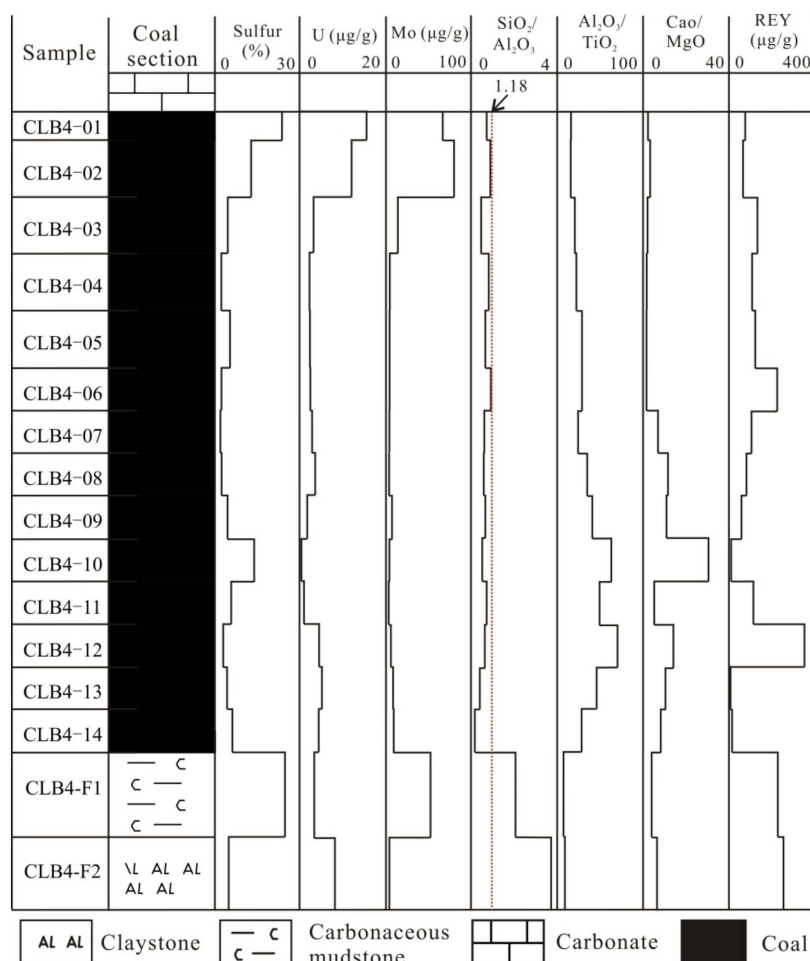
Figure 5. Vertical distribution of sulfur, U, Mo, REY, SiO_2/Al_2O_3, Al_2O_3/TiO_2, and CaO/MgO (on whole-coal basis).

4.2. Minerals in the Coal and Floor Samples

The contents of crystalline mineral phases in the coal and floor samples are given in Table 2. XRD analysis shows that mineral matter in the C4 Coal is dominated mainly by pyrite and, to a lesser extent, tobelite, kaolinite, and calcite, along with traces of marcasite in several coal benches as well. Quartz and svanbergite are only present in sample CLB4-1 and CLB4-12, respectively (Figure 3).

Mineral matter of floor sample CLB4-F1 is dominated by pyrite and kaolinite, and, to a lesser extent, quartz, while that of floor sample CLB4-F2 is composed primarily of kaolinite and quartz, with a lesser amount of pyrite (Figure 3).

Other mineral phases including apatite, Al-oxyhydroxide minerals, and Fe-sulfate, although below the detection limit of XRD analysis, were also identified by SEM-EDS analysis.

Table 2. Mineralogical proportions of the coal and floor samples determined by X-Ray Diffraction (XRD) from the Chalinbao underground coal mine in the Tongzi Coalfield (on whole-coal basis; unit in%).

Sample	Kaolinite	Quartz	Calcite	Pyrite	Marcasite	Tobelite	Svanbergite	Anatase	Gypsum
CLB4-1	<dl	2.0	<dl	38.2	<dl	<dl	<dl	<dl	<dl
CLB4-2	4.4	<dl	<dl	17.0	0.4	<dl	<dl	<dl	<dl
CLB4-3	3.2	<dl	<dl	9.8	0.8	0.3	<dl	<dl	<dl
CLB4-4	2.9	<dl	<dl	3.8	0.5	3.5	<dl	<dl	<dl
CLB4-5	2.6	<dl	<dl	12.4	<dl	4.6	<dl	<dl	<dl
CLB4-6	2.5	<dl	<dl	3.5	<dl	4.9	<dl	<dl	<dl
CLB4-7	<dl	<dl	2.3	3.1	<dl	4.3	<dl	<dl	<dl
CLB4-8	<dl	<dl	2.5	2.4	<dl	3.3	<dl	<dl	<dl
CLB4-9	<dl	<dl	0.6	7.0	<dl	3.2	<dl	<dl	<dl
CLB4-10	<dl	<dl	3.9	18.9	<dl	1.6	<dl	<dl	<dl
CLB4-11	<dl	<dl	<dl	9.9	<dl	5.4	<dl	<dl	<dl
CLB4-12	1.6	<dl	<dl	4.6	<dl	5.8	4.6	<dl	<dl
CLB4-13	<dl	<dl	0.4	5.9	<dl	1.1	<dl	<dl	<dl
CLB4-14	<dl	<dl	<dl	8.5	<dl	0.4	<dl	<dl	<dl
CLB-F1	12.4	14.8	<dl	45.6	<dl	<dl	<dl	<dl	<dl
CLB-F2	44.0	39.4	2.1	10.6	<dl	<dl	<dl	1.9	2.0

<dl, below detection limit.

4.2.1. Pyrite

Pyrite is the predominant constituent both in the coal and floor samples. Pyrite content fluctuates considerably throughout the C4 Coal and reaches the highest one in the coal bench immediately underlying the marine limestone (Figure 3). Pyrite is present in several forms in the C4 Coal, mainly as isolated euhedral crystals embedded in the organic matrix (Figure 6A), aggregates of individual crystals (Figure 6B), and cell lumen-fillings (Figure 6C,D), all of which indicate an approximately contemporaneous early diagenetic formation.
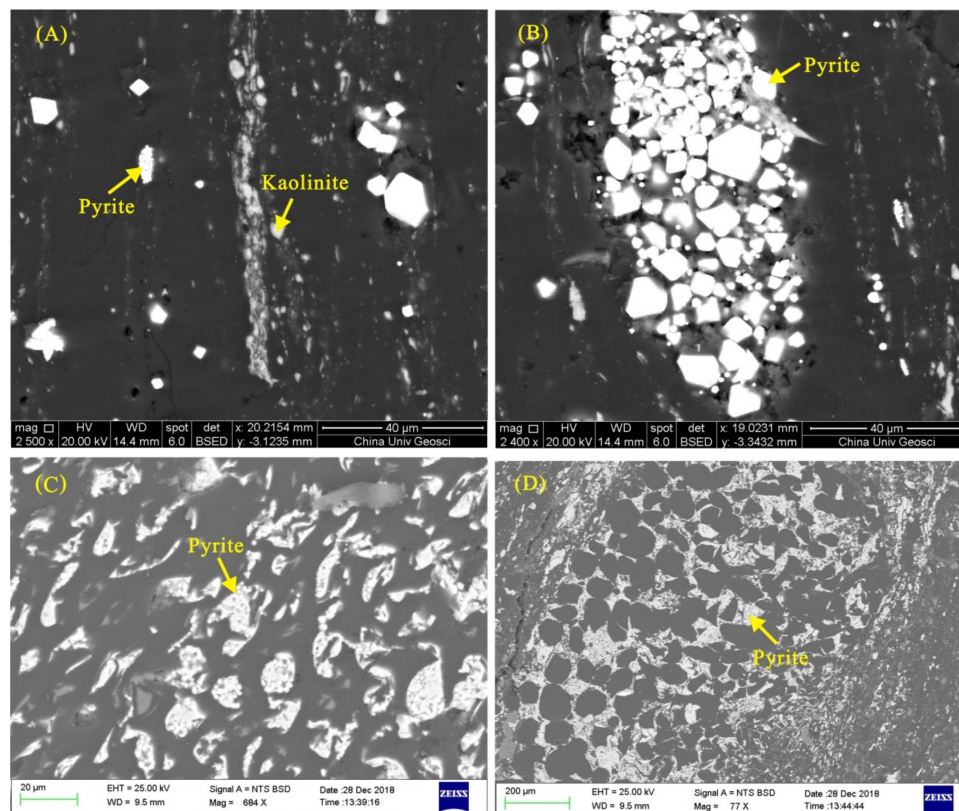
Figure 6. Scanning electron microscope (SEM) back-scattered electron images of minerals in the C4 Coal. (**A**): isolated pyrite and kaolinite grains (sample CLB4-12); (**B**): euhedral pyrite aggregate (sample CLB4-12); (**C**) and (**D**): cell-filling pyrite (sample CLB4-2).

Pyrite in the floor samples is present as visible lenticles or nodules (0.5–10 cm in size) in hand specimen. It is also found as massive forms (Figure 7F) and sub-euhedral crystals distributed into the kaolinite matrix (Figure 7G) under SEM-EDS analysis, all of which appear to be essentially of early diagenetic origin.
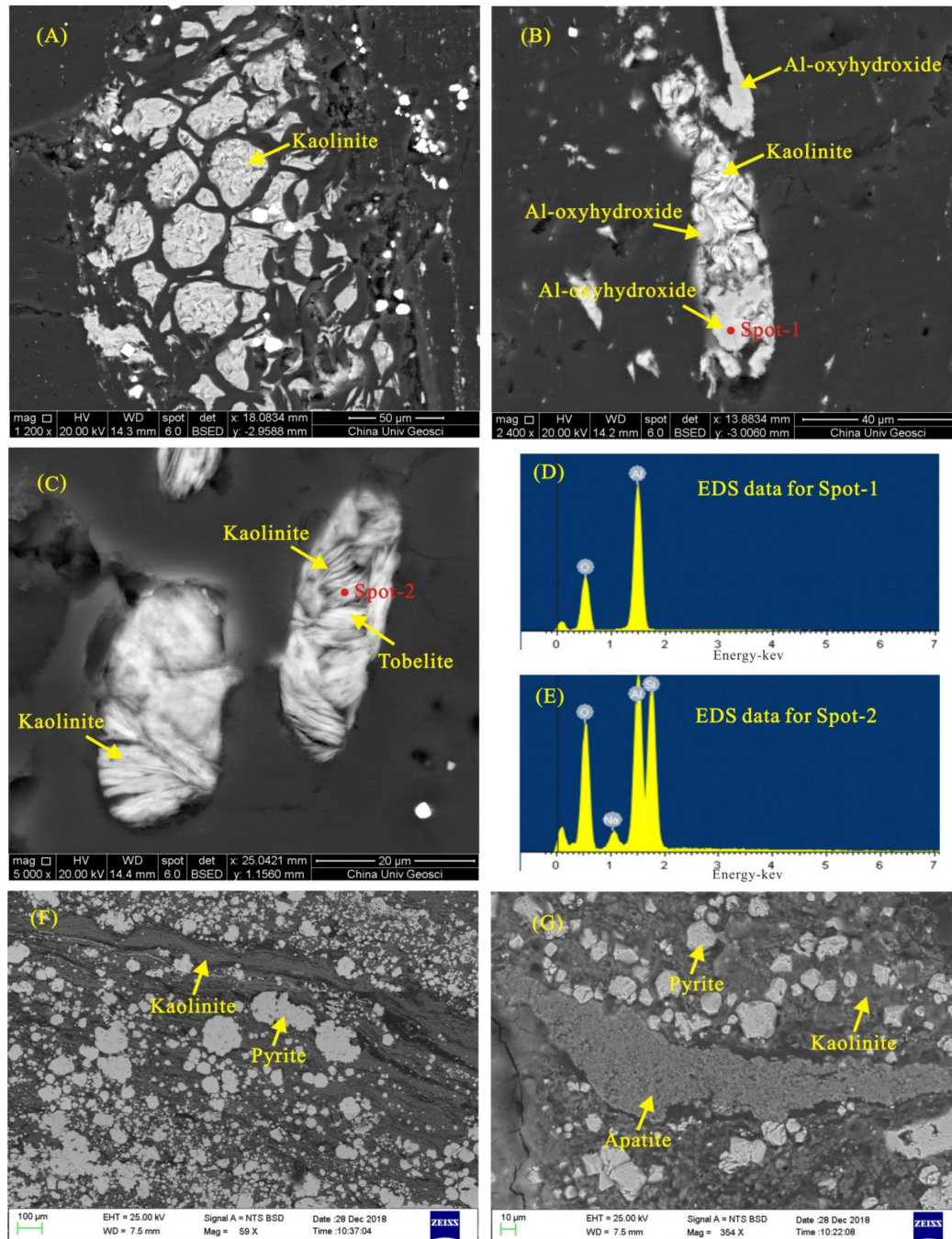

Figure 7. SEM back-scattered electron images of minerals in coal (sample CLB4-12) and floor (sample CLB4-F1) samples and energy-dispersive X-ray spectrometer (EDS) analysis of selected minerals. (**A**): cell-filling kaolinite; (**B**): kaolinite, along with Al-oxyhydroxide minerals, occurring as pore space infillings; (**C**): intergrowth of kaolinite and tobelite; (**D**): EDS spectra of Al-oxyhydroxide minerals; (**E**): EDS spectra of kaolinite containing traces of Na; (**F**): massive pyrite and kaolinite matrix; (**G**): massive pyrite, kaolinite matrix, and lath-like apatite.

4.2.2. Kaolinite

A minor amount of kaolinite is present mainly in the upper coal benches (Figure 3). Kaolinite is present as cell-fillings (Figure 7A–C), apparently indicating an authigenic origin. The rounded kaolinite grains are distributed along the bedding planes (Figure 8A), appearing to be of terrigenous detrital origin. The SEM-EDS data show that the cell-filling kaolinite, in some instances, contains traces of Na (Figure 7E).

Kaolinite in the floor samples occurs mostly as kaolinite matrix (Figure 7F,G). In a few cases, kaolinite is present as fracture infillings alongside the outer edge of quartz infillings (Figure 9C).
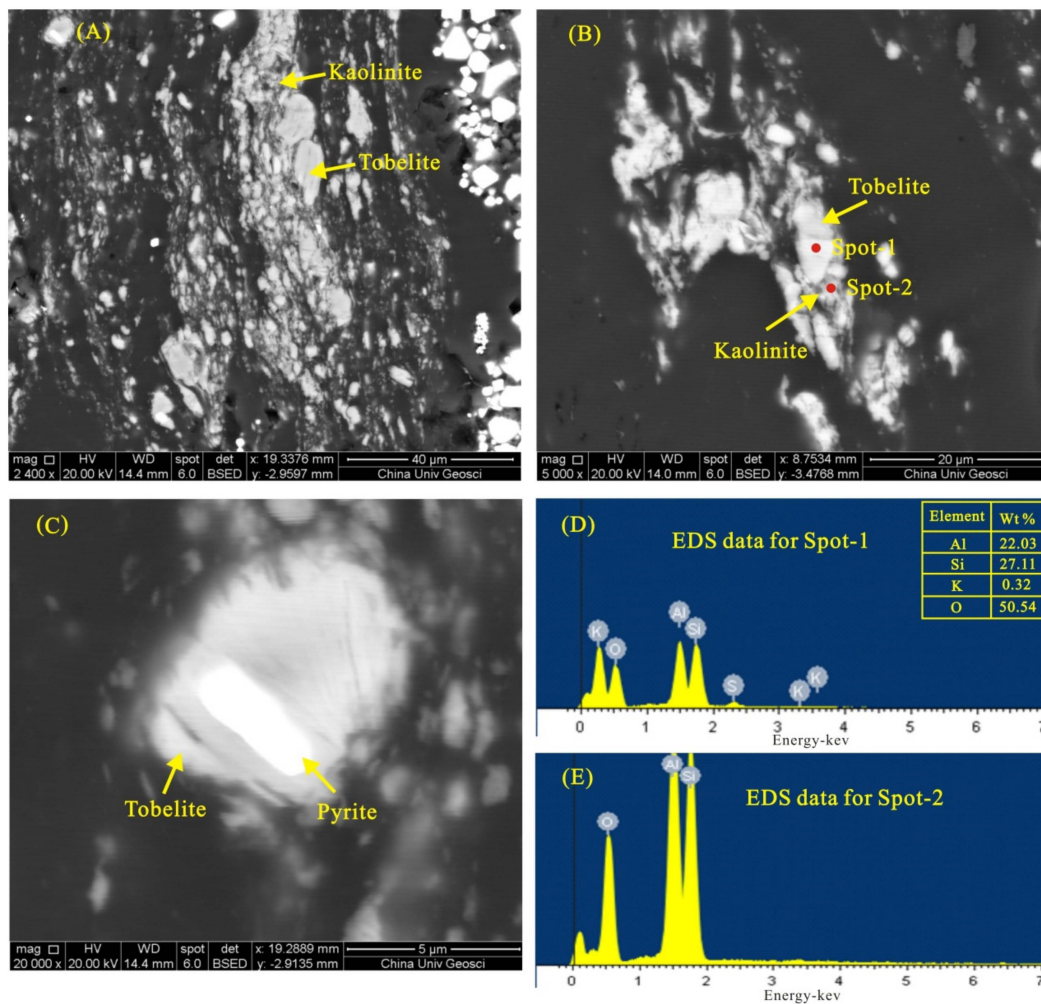

Figure 8. SEM back-scattered electron images of minerals in the coal sample (sample CLB4-12) and EDS analysis of selected minerals. (**A**): dispersed kaolinite and tobelite particles along bedding planes; (**B**): pore space-filling tobelite; (**C**): pore space-filling tobelite containing an inclusion of pyrite; (**D**): EDS spectra of tobelite containing trace K; (**E**): EDS spectra of kaolinite.
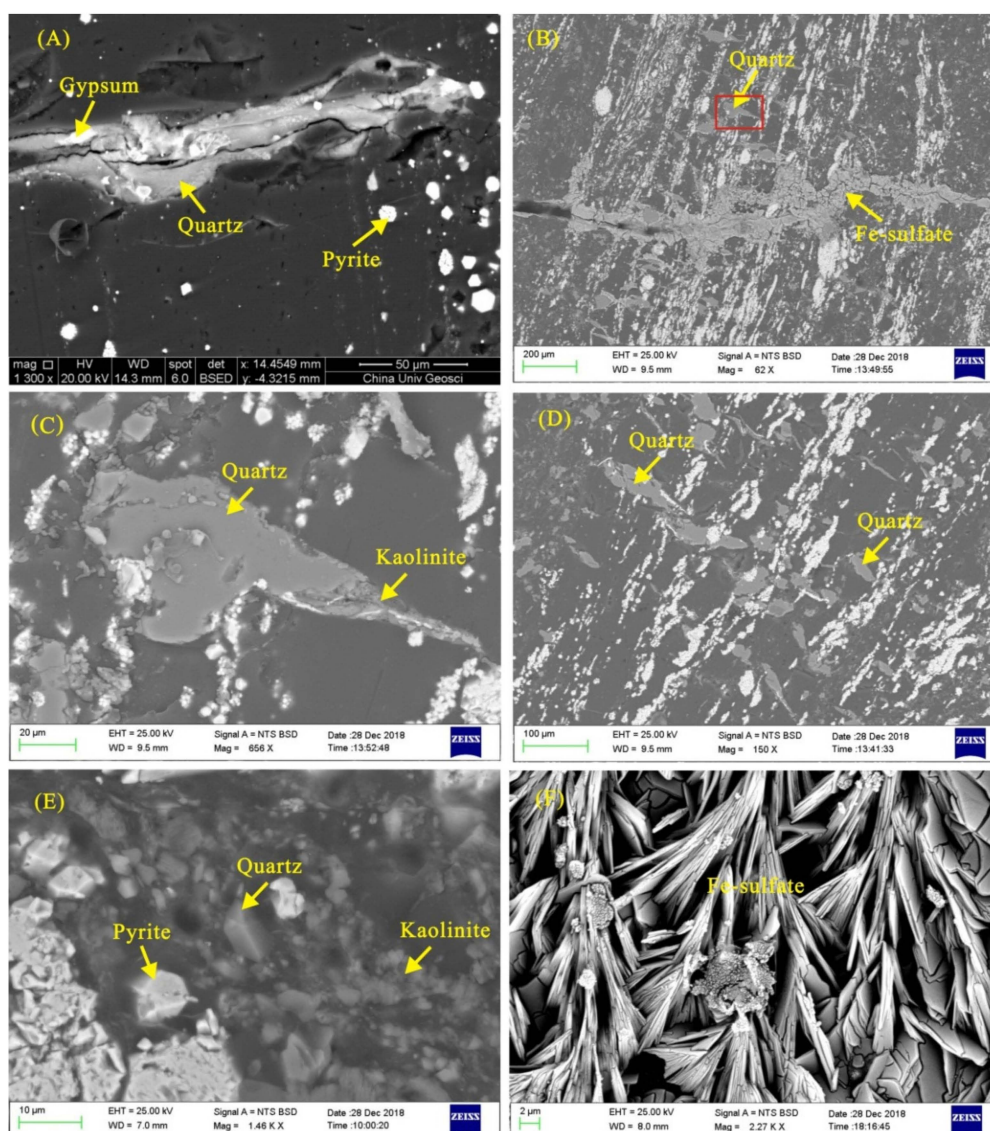
Figure 9. SEM back-scattered electron images of minerals in the coal sample (sample CLB4-12) and floor sample (sample CLB4-F1). (**A**): fracture-filling quartz and gypsum; (**B**): fracture-filling quartz and Fe-sulfate; (**C**): fracture-filling quartz, with kaolinite occurring along the outer edge of quartz; (**D**): fracture-filling quartz; (**E**): kaolinite matrix, dispersed pyrite particle, and euhedral quartz grain; (**F**): needle-like Fe-sulfate.

4.2.3. Tobelite

Tobelite (or ammonium-bearing illite) in the C4 Coal is identified by the XRD diffraction peak. Alternatively, the higher NH_4^+ concentration in sample CLB4-5+6 than in sample CLB4-2 (Table 3) also further confirms the XRD result that tobelite is present in sample CLB4-5 and CLB4-6 but below the XRD detection limit in sample CLB4-2 (Figure 3). Moreover, a good linear relationship between NH_4^+ and tobelite is observed in Figure 4C, also supporting the presence of NH_4^+-bearing mineral phases. The exchangeable NH_4^+ contents in the selected samples are listed in Table 3. The concentration of NH_4^+ in sample CLB4-5+6 and CLB4-2 ranges from 14.14 to 35.54 µg/g and from 1.63 to 2.11 µg/g, respectively, indicating a higher NH_4^+ concentration in the former than the latter. According to the tobelite content in the samples and the maximum NH_4^+ exchangeable contents, NH_4^+ contents in tobelite might reach 0.076%, which is much lower than the 3.2% stoichiometric content of NH_4^+ in

tobelite in the case where NH_4^+ is the only cation of the clay. Thus, relevant proportions of K^+ or Na^+ should be present in this case.

Tobelite occurs abundantly in the middle coal benches but below the detection limit of XRD analysis at the top of the C4 Coal (Figure 3). Tobelite primarily occurs as rounded particles embedded into the organic matrix or kaolinite matrix (Figure 8A), pore space infillings (Figure 8B,C), and cell filings (Figure 7C). The tobelite has a higher brightness than kaolinite in the BES images (Figures 7C and 8A–C) and contains traces of K (0.32% on average) in the spectra (Figure 8D). Dai et al. [22] and Zhao et al. [48] also indicated that K^+ in trace amount is also present in tobelite. In contrast, kaolinite that is intimately associated with tobelite does not show K peak at all in the spectra (Figure 8E).

Table 3. Concentration of NH_4^+ in sample CLB4-5+6 (a mixture of sample CLB4-5 and CLB4-6) and CLB4-2.

Sample	Weight (g)	Volume (mL)	NH_4^+ (mg/L)	NH_4^+ (µg/g)
CLB4-5+6	0.5002	25	0.283	14.14
CLB4-5+6	0.5010	50	0.231	23.05
CLB4-5+6	0.5093	25	0.306	15.02
CLB4-5+6	0.5018	50	0.239	23.81
CLB4-5+6	0.2504	50	0.178	35.54
CLB4-2	0.5074	25	0.033	1.63
CLB4-2	0.5031	50	0.020	1.99
CLB4-2	0.5072	25	0.038	1.87
CLB4-2	0.5030	50	0.021	2.11

4.2.4. Quartz

Quartz is only present in the uppermost coal bench immediately underneath the marine limestone in minor amounts but is abundant in the floor samples (Figure 3). The majority of quartz is in the form of fracture infillings and, in some cases, it is associated with gypsum in the coals (Figure 9A), indicating an epigenetic origin.

In the floor samples, quartz is present mainly as the fracture/cleat infillings (Figure 9B–D) mostly perpendicular to the bedding planes, indicating epigenetic precipitation from the Si-rich solutions migrating along the permeable fractures. Quartz is also present as euhedral crystals (Figure 9E), analogous to that of volcanic origin, as indicated by Wang et al. [49].

4.2.5. Sulfate Minerals

Gypsum is present as fracture infillings in the C4 coals (Figure 9A) and probably originates as a weathering product arising from the interaction of calcite with SO_4^{2-} derived from the pyrite oxidation [3,50,51]. Fe-sulfate was also observed in the coal and floor samples and occurs mainly as fracture infillings (Figure 9B,F). The Fe-sulfate and pyrite are often spatially associated (Figure 9B), probably indicating its derivation from the oxidation of pyrite. However, the euhedral needle-like Fe-sulfate crystals with good crystallization (Figure 9F) could have precipitated from the migrating solutions.

4.2.6. Calcite

Calcite in minor amounts is mainly distributed in the middle coal benches (Figure 3). The bulk of calcite is in the form of fracture infillings perpendicular or inclined to the bedding planes (Figure 10A,B), apparently indicating epigenetic precipitation from Ca-rich migrating solutions after the coal was completely compacted [51]. The SEM-EDS mapping shows (Figure 10) that the fracture-filling veins mostly consist of calcite (Figure 10B) and a lesser amount of quartz (Figure 8C), along with traces of Al-oxyhydroxide minerals (Figure 10D).
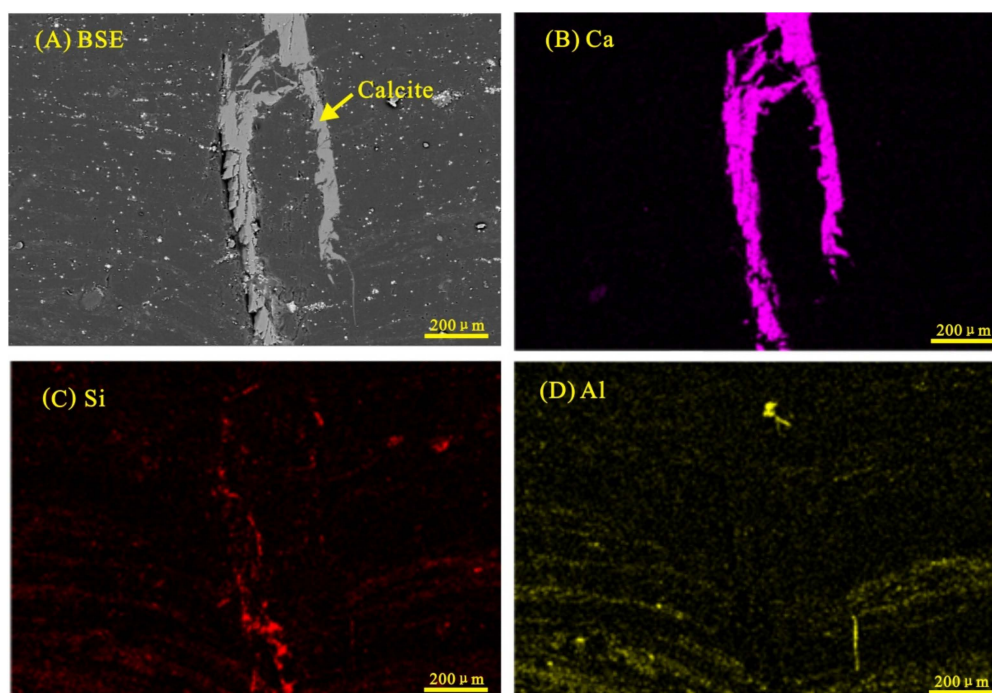
Figure 10. SEM-EDS mapping showing the distribution of Ca, Si, and Al (sample CLB4-7). (**A**): SEM back-scattered electron images of minerals; (**B**)–(**D**): the distribution of Ca, Si, and Al, respectively.

4.2.7. Al-Oxyhydroxide Minerals

The Al-oxyhydroxide minerals, possibly boehmite or diaspore, were also identified by the SEM-EDS analysis. The Al-oxyhydroxide minerals occur, along with kaolinite, as cell-fillings (Figure 7B,D) and, in a few instances, as fracture infillings associated with calcite and quartz (Figure 10D), all of which appear to be a result of authigenic precipitation from Al-rich solutions. In some cases, Al-oxyhydroxide minerals are found as disseminated fine-grained particles along the bedding planes (Figure 10D), indicative of a terrigenous detrital origin. The co-existence of Al-oxyhydroxide minerals and quartz (Figure 10) suggests that the solutions involved in the formation of them were introduced at various coalification stages: otherwise, Si and Al in solutions will react to form kaolinite.

4.3. Geochemistry

The concentrations of major-element oxides and trace elements in the C4 coal and floor samples from the Chalinbao underground coal mine in the Tongzi Coalfield are tabulated in Table 4.

Table 4. Major-element oxides (%) and trace element concentrations (μg/g) of the coal and floor samples from the Chalinbao underground coal mine in the Tongzi Coalfield (on whole-coal basis).

Sample	CLB 4-1	CLB 4-2	CLB 4-3	CLB 4-4	CLB 4-5	CLB 4-6	CLB 4-7	CLB 4-8	CLB 4-9	CLB 4-10	CLB 4-11	CLB 4-12	CLB 4-13	CLB 4-14	CLB -F1	CLB -F2
SiO_2	1.96	2.06	1.66	3.06	3.50	3.58	2.14	1.61	1.60	0.78	2.66	3.61	0.53	0.18	17.17	58.95
TiO_2	0.15	0.13	0.15	0.15	0.18	0.13	0.13	0.07	0.06	0.02	0.07	0.08	0.03	0.03	0.93	1.52
Al_2O_3	2.60	2.21	3.36	3.58	5.09	3.76	3.31	2.63	2.33	1.46	3.50	5.42	1.25	0.92	7.96	16.18
Fe_2O_3	29.59	15.06	4.74	1.36	5.62	1.51	0.93	1.26	4.19	16.60	5.67	2.14	3.72	6.26	35.29	9.79
MgO	0.04	0.03	0.06	0.06	0.09	0.07	0.06	0.05	0.04	0.04	0.07	0.05	0.02	0.03	0.13	0.20
CaO	0.08	0.09	0.10	0.09	0.07	0.09	0.43	0.51	0.41	1.06	0.34	0.72	0.24	0.20	0.48	1.30
Na_2O	0.02	0.03	0.04	0.05	0.06	0.04	0.03	0.03	0.03	0.02	0.05	0.05	0.05	0.06	0.11	0.24
K_2O	0.07	0.04	0.08	0.10	0.19	0.10	0.10	0.06	0.05	0.04	0.14	0.08	0.03	0.04	0.19	0.42
Li	17	13	35	35	52	48	46	40	25	10	30	40	5.5	2.2	49	76
Be	<dl	1.9	3.1	2.9	2.6	3.1	3.8	3.2	3.0	2.0	3.2	4.8	1.6	1.6	0.92	1.2
P	166	99	93	57	312	636	66	57	67	48	1536	9753	220	816	1092	131
B	2.0	6.0	1.0	13	15	7.3	17	29	18	7.0	32	41	22	16	28	19
Sc	2	<dl	<dl	<dl	<dl	<dl	<dl	<dl	<dl	<dl	<dl	<dl	<dl	<dl	8.2	9.7

Table 4. *Cont.*

Sample	CLB 4-1	CLB 4-2	CLB 4-3	CLB 4-4	CLB 4-5	CLB 4-6	CLB 4-7	CLB 4-8	CLB 4-9	CLB 4-10	CLB 4-11	CLB 4-12	CLB 4-13	CLB 4-14	CLB -F1	CLB -F2
V	106	39	24	22	19	16	21	29	29	10	18	26	27	21	144	237
Cr	20	9.2	13	12	10	8.3	10	11	10	2.6	6.9	12	15	13	97	175
Mn	58	23	8.8	9.0	9.0	9.5	45	36	47	106	26	26	21	10	697	20
Co	26	2.4	2.5	1.3	2.1	1.6	2.4	2.3	6.1	9.2	14	19	8.4	15	47	15
Ni	64	9.4	6.9	5.6	8.5	8.0	7.1	6.4	7.4	6.6	13	17	10	13	40	57
Cu	31	18	12	8.7	25	13	11	11	14	27	25	24	14	18	59	83
Zn	4.2	26	12	29	6.9	28	16	7.3	6.8	19	11	46	39	76	47	77
Ga	3.9	4.9	5.4	5.1	6.1	6.0	5.0	4.1	3.4	2.6	6.2	5.0	1.8	2.3	18	17
Ge	1.2	3.2	3.0	4.1	4.5	1.7	1.7	6.2	7.2	3.4	11	17	22	18	1.2	1.0
As	18	17	4.6	2.7	11	2.4	1.9	2.0	3.7	18	4.9	6.5	6.9	5.3	24	9.3
Se	15	19	10	5.6	19	6.8	4.3	3.9	5.0	16	8.3	13	7.7	6.2	20	11
Rb	1.2	0.8	1.8	2.2	4.7	2.0	2.2	<dl	<dl	<dl	4.2	1.5	<dl	1.1	4.8	8.3
Sr	84	84	81	87	197	365	90	89	87	97	590	3947	83	76	104	104
Y	10	7.5	13	14	14	16	21	13	8.5	3.6	8.7	34	3.5	5.7	25	21
Zr	119	38	83	52	103	109	163	47	32	8.9	24	128	17	10	332	326
Nb	7.2	5.1	12	7.9	18	20	21	7.7	3.4	1.2	6.2	26	2.5	1.1	44	49
Mo	67	80	14	4.9	4.7	4.7	3.2	3.5	7.5	4.3	3.7	6.1	7.8	9.4	53	4.3
Sn	1.4	<dl	<dl	<dl	<dl	<dl	<dl	<dl	<dl	<dl	<dl	<dl	<dl	<dl	5.3	4.0
Cs	<dl	<dl	<dl	<dl	<dl	<dl	<dl	<dl	<dl	<dl	<dl	<dl	<dl	<dl	0.52	0.90
Ba	32	6.1	13	15	28	21	17	7.9	6.3	6.5	16	36	3.8	5.4	27	20
La	15	16	25	21	28	55	17	14	8	1.4	29	75	0.9	1.5	48	65
Ce	29	25	54	40	47	95	35	30	20	3.5	48	136	2.0	3.8	88	99
Pr	2.9	2.4	6.0	4.4	5.0	9.6	3.9	3.2	2.2	<dl	4.6	15	<dl	<dl	9.3	11
Nd	10	8.5	22	16	18	33	15	13	8.5	1.8	15	60	1.0	2.2	33.6	35.9
Sm	2.0	1.7	4.7	3.5	3.1	5.1	3.3	2.9	2.0	<dl	2.6	12	<dl	<dl	6.2	5.4
Eu	<dl	<dl	<dl	<dl	<dl	0.68	<dl	<dl	<dl	<dl	0.36	0.9	<dl	<dl	1.0	1.0
Gd	1.9	1.7	3.7	3.1	2.7	3.7	3.3	2.6	1.7	<dl	2.3	9.4	<dl	1.0	5.4	5.0
Tb	<dl	<dl	<dl	<dl	<dl	0.79	<dl	<dl	<dl	<dl	0.42	1.07	<dl	<dl	0.80	0.81
Dy	2.0	1.3	2.4	2.4	2.4	2.7	3.3	2.1	1.3	<dl	1.4	5.3	<dl	0.8	4.5	5.2
Ho	<dl	<dl	<dl	<dl	<dl	0.71	<dl	<dl	<dl	<dl	0.37	0.97	<dl	<dl	0.86	0.99
Er	1.3	0.83	1.5	1.4	1.6	1.7	2.2	1.2	0.89	<dl	0.88	3.1	<dl	<dl	2.5	2.7
Tm	<dl	<dl	<dl	<dl	<dl	<dl	<dl	<dl	<dl	<dl	<dl	<dl	<dl	<dl	0.36	0.40
Yb	1.5	0.82	1.4	1.3	1.6	1.7	2.2	1.2	0.92	<dl	0.92	3.0	<dl	<dl	2.4	2.7
Lu	<dl	<dl	<dl	<dl	<dl	<dl	<dl	<dl	<dl	<dl	<dl	<dl	<dl	<dl	0.34	0.38
Hf	1.7	1.0	2.3	1.5	2.8	2.9	4.3	1.3	0.90	0.25	0.62	3.5	0.46	0.29	7.7	9.1
Ta	<dl	<dl	<dl	<dl	<dl	<dl	0.79	<dl	<dl	<dl	<dl	<dl	<dl	<dl	2.6	2.8
Tl	0.78	<dl	<dl	<dl	<dl	<dl	<dl	<dl	<dl	<dl	<dl	<dl	<dl	<dl	0.15	0.10
Pb	8.3	13	6.8	2.6	12	4.6	2.2	2.1	3.7	14	2.8	4.1	2.4	1.9	19	21
Th	2.0	2.3	4.0	3.6	7.1	4.1	4.8	2.2	1.3	<dl	0.93	3.1	<dl	<dl	9.9	14
U	16	12	3.3	2.4	2.5	2.5	3.0	3.7	1.8	0.51	1.1	4.6	5.3	4.5	3.5	8.3

<dl, below detection limit.

4.3.1. Major-Element Oxides

Fe_2O_3 is the dominant oxide, with minor Al_2O_3 and SiO_2 and lesser amounts of K_2O, Na_2O, MgO, CaO, and TiO_2, as expected from the mineralogical compositions that are dominated by pyrite and, to a lesser extent, tobelite and kaolinite. In comparison to studies of Chinese coals by Dai et al. [1], the contents of major-element oxides, except for Fe_2O_3, are significantly lower than the corresponding averages of the Chinese coals, mainly due to low ash yield in the C4 Coal. The Fe_2O_3 content is 1.5 times higher in the C4 Coal than in Chinese coals, due to higher pyrite amounts. The SiO_2/Al_2O_3 ratio ranges from 0.19 to 0.95, with an average of 0.66 that is markedly lower than the theoretical ratio of kaolinite (1.18) (Figure 5), primarily due to the presence of Al-oxyhydroxide minerals, as shown in Figures 7B and 10D.

The content of Fe_2O_3 in the C4 Coal shows a significant linear relationship with ash yield (r = 0.93, Figure 4D), suggesting that iron-bearing mineral phases, mostly pyrite, contributes significantly to the overall ash yield, as indicated also by the positive correlation of pyrite-ash yield (r = 0.95, Figure 4E). Additionally, the interception on the ash yield axis is approximately 6.4% (Figure 4E), indicating that other mineral phases may contribute to 6.4% of ash yield, which is in turn supported by the total non-sulfides minerals content of 5.1%. The significant correlations of Fe–S (r = 1.00, Figure 4F), Fe-pyrite (r = 0.98, Figure 4G), and S-pyrite (r = 0.98, Figure 4H) confirm that both Fe and S are mostly

incorporated into pyrite. Iron is plotted as a function of S in Figure 4F, where the interception on the S axis (Figure 4F) indicates approximately 1.62% organic and/or sulfate-S content. CaO is primarily hosted in calcite, as evidenced by the correlation of CaO-calcite (r = 0.88, Figure 4I). Moreover, the CaO/MgO ratio is higher in the lower coal benches than in the upper ones (Figure 5), consistent with the presence of calcite (Figure 3). A good linear relationship between K_2O and Al_2O_3 (r = 0.79; Figure 4J) is also observed, probably suggesting that K_2O is hosted mainly within aluminosilicate minerals, most likely tobelite, as attested by the relatively significant correlation of K_2O-tobelite (r = 0.66; Figure 4K) and SEM-EDS spectrum showing the presence of K peak in tobelite (Figure 8D).

4.3.2. Trace Elements

The concentration coefficient (CC = trace element concentration in sample/referenced coal Clark reported by Ketris and Yudovich [52]) is used to better discriminate the degree of enrichment or depletion of trace elements in coals [53]. In comparison with world hard coals [52], Se and Mo are enriched (5.0 < CC < 10.0) in the C4 Coal; Li, P, Ge, Sr, Nb, La, and U are slightly enriched (2.0 < CC < 5.0); the contents of other trace elements are either similar to (0.5 < CC <2.0) or apparently lower (CC < 0.5) (Figure 11A). Compared with the trace-element averages of Western Guizhou coals [16], Se is enriched; P and Sr are slightly enriched; the remaining trace elements are close to or lower (Figure 11B).
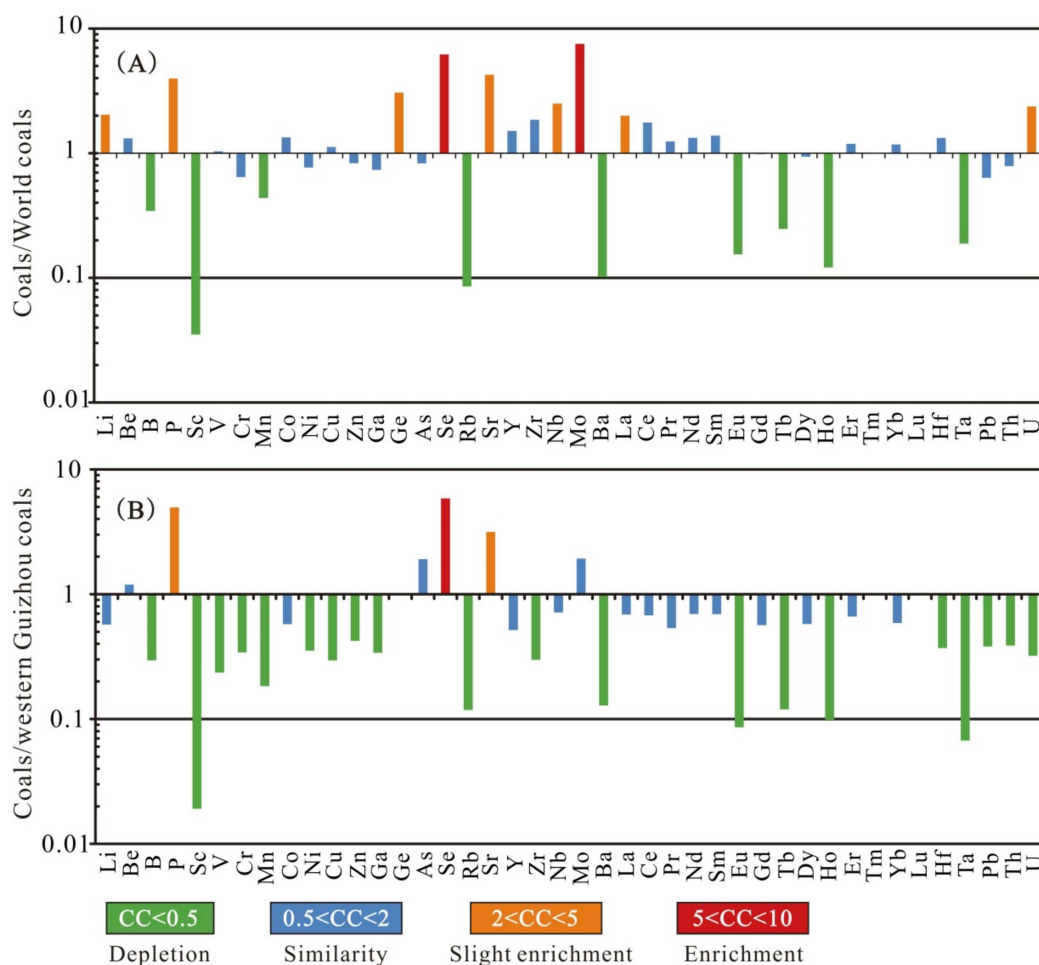

Figure 11. Concentration coefficients (CC) of trace elements in the study coals, normalized to the respective average of world coal (**A**) [52] and western Guizhou coal (**B**) [16].

The elevated concentrations of Mo, Se, and U in the C4 coals most likely occur in the pyrite, as evidenced by the SEM-EDS mapping (Figure 12), where Fe, S, Mo, Se, and U show a similar distribution

(Figure 12). In addition, U and Mo are apparently enriched in the coal benches directly underlying the marine limestone (Figure 5), appearing to indicate that seawater diffusion into the underlying C4 Coal plays a vital role in their enrichment. The slightly elevated Sr and P contents are only caused by sample CLB4-12, which contains anomalously high Sr and P contents (Table 4) due to the occurrence of svanbergite as evidenced by XRD analysis (Figure 3).
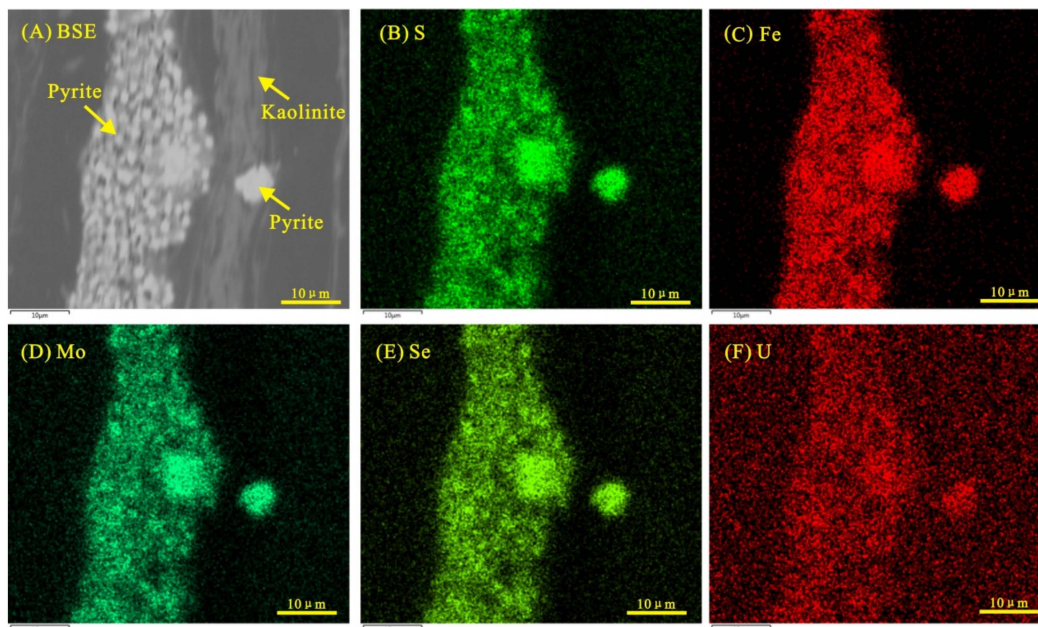

Figure 12. SEM-EDS mapping showing the distribution of S, Fe, Mo, Se, and U (sample CLB4-1). (**A**): SEM back-scattered electron images of minerals; (**B**)–(**F**): the distribution of S, Fe, Mo, Se, and U, respectively.

4.3.3. Rare Earth Elements and Yttrium (REY)

Seredin and Dai [54] have proposed a classification and enrichment types of REEs and Y (REY) adopted in the present study. By a comparison to Upper Continental Crust (UCC) [55], three REY distribution patterns can be distinguished, including L-REY type, M-REY type, and H-REY type [54]. The contents of REY in the coals range from 7.4 to 355 µg/g, with an average of 105 µg/g that is slightly higher than the average for world hard coals (68 µg/g [52]), but somewhat lower than the average of Chinese coals (136 µg/g [1]). The highest REY content (355 µg/g) in sample CLB4-12 (Figure 5) is accompanied by the highest phosphorus content (9753 µg/g) and by the presence of svanbergite (Figure 3), indicating that the elevated REY concentration is primarily hosted within phosphate minerals such as svanbergite. Aside from the carrier of phosphate minerals, a good linear relationship between REY and Al_2O_3 was also observed (Figure 4L), suggesting that the aluminosilicate mineral assemblages may also be the host of REY.

The plot of UCC-normalized REY patterns in the C4 Coal shows an L-REY distribution type and strongly negative Eu anomaly (Figure 13A). The floor samples, however, have an L-REY distribution type and a slightly negative Eu anomaly (Figure 13B). The coals have a similar REY distribution, indicating that the REY may have been derived from similar detrital materials [56] or tectonic setting [57].
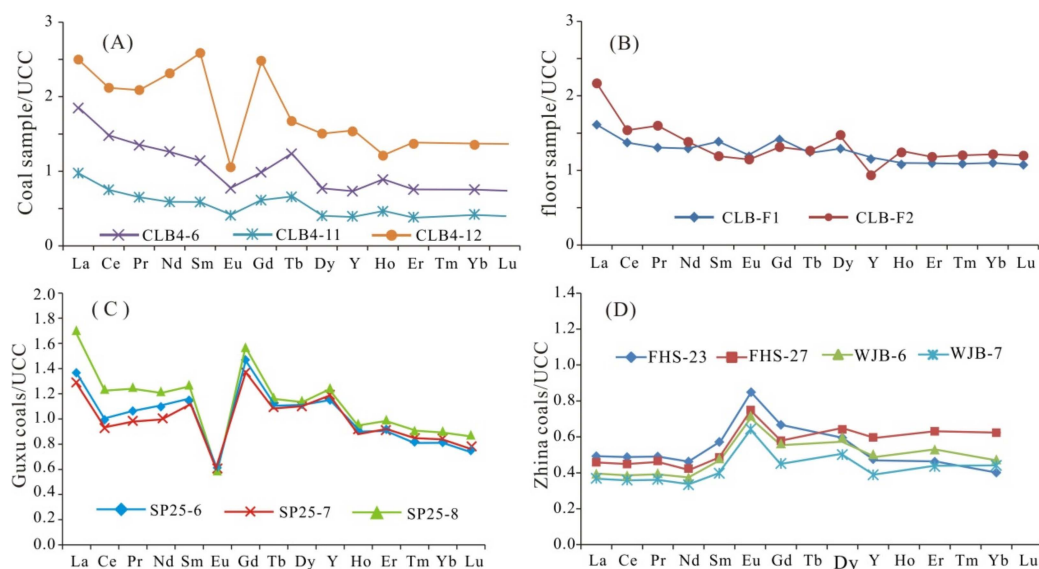
Figure 13. Distribution patterns of rare earth elements and yttrium (REY) in the study coals (**A**), floor rocks (**B**), Guxu coals (**C**) [21], and Zhina coals (**D**) [12]. REY are normalized to Upper Continental Crust [55].

5. Discussion

5.1. Marine Influence

Previous studies have indicated that the coals subjected to marine influence contain higher S content than those formed in freshwater environments [47]. However, elevated S in coals might be also the result of the influx of hydrothermal fluids or pyroclastic materials [18,58] or syn-sedimentary high S-freshwaters due to leaching of high sulfate source rocks [59]. In the present study, the high S content (7.0% on average), combined with the occurrence of macroscopical pyrite nodules and bands as well as microscopic early diagenetic pyrite crystals (Figure 6A–D) in the C4 Coal and floor samples, clearly indicates a marine-influenced coal-forming environment, which is in turn supported by Shao et al. [7] who reported that the Late Permian strata in the Tongzi coalfield were formed in a neritic shelf environment or carbonate platform environment. Moreover, the fact that the C4 Coal is directly overlain by the marine limestone (Figure 2) also confirms a contribution from seawater circulation.

The various degrees of seawater diffusion into peat swamp may have resulted in variation in mineralogical and geochemical patterns throughout the C4 Coal. The uppermost coal bench (sample CLB4-1) immediately underneath the marine limestone has the highest pyrite, S, Fe, V, Co, Ni, U, and Mo contents compared to other coal benches. A comparison of elements abundances in the high-S coals with those in the medium-S coals shows that some elements with a sulfide affinity (e.g., Fe, S, Co, Ni, As, Se, Mo, U, and Pb) are higher in the high-S coals than in the medium-sulfur coals, indicating that the seawater circulation plays a vital role in these elements distribution. In addition, some amounts of U and Mo are probably derived from other sources in the U- or Mo-rich coal benches (Figure 5), because claystone in the Qianbei Upland is considered as possible detrital material, as discussed below, that was subjected to intense chemical weathering and leaching, resulting in the loss of some mobile elements such as U and Mo, as reported by Marynowski et al. [60].

5.2. Sediment-Source Region

Prior studies have shown that terrigenous detrital materials for the Late Permian coals in Guizhou Province were derived from the Kangdian Upland that consists predominantly of the Emeishan basalts, along with the Emeishan felsic rocks at the uppermost part of the Kangdian Upland [6,10,28,36]. The Late Permian coals that have been derived from the Kangdian Upland Emeishan basalts are commonly

enriched in transition metal elements such as Sc, V, Cr, Co, and Ni [16,19,61] because they are commonly enriched in the Emeishan basalts [1,6,9,19,62]. However, these trace elements in the C4 Coal are either comparable to or even lower than the corresponding averages for Western Guizhou coals [16], possibly indicating that the coals are not deriving from the Emeishan basaltic detrital materials.

It has been reported that Al_2O_3/TiO_2 ratio is a reliable geochemical index in inferring parent rock compositions in sedimentary rocks [63,64], along with 3–8, 8–21, and 21–70 indicative for mafic, intermediate, and felsic compositions, respectively [63]. This index is also widely used in recent studies to monitor the nature of sediment-source rocks for some coal deposits [11,65–68]. In the present study, the Al_2O_3 is ploted as a function of TiO_2 in Figure 14, where the C4 coals mostly fall into the area of felsic rocks and floor samples fall within the low-Ti basalt area (Figure 14). Alternatively, the Al_2O_3/TiO_2 values (36 on average) in the C4 Coal are comparable to that in the Emeishan felsic rocks (31 on average) at the top of the Kangdian Upland [10,32,33]. This appears to indicate terrigenous source materials with felsic compositions. Moreover, the Al_2O_3/TiO_2 ratio decreases from the lower part towards the upper part of the C4 Coal (Figure 5), probably indicating a progressively decreasing input of felsic-dominated detrital materials.
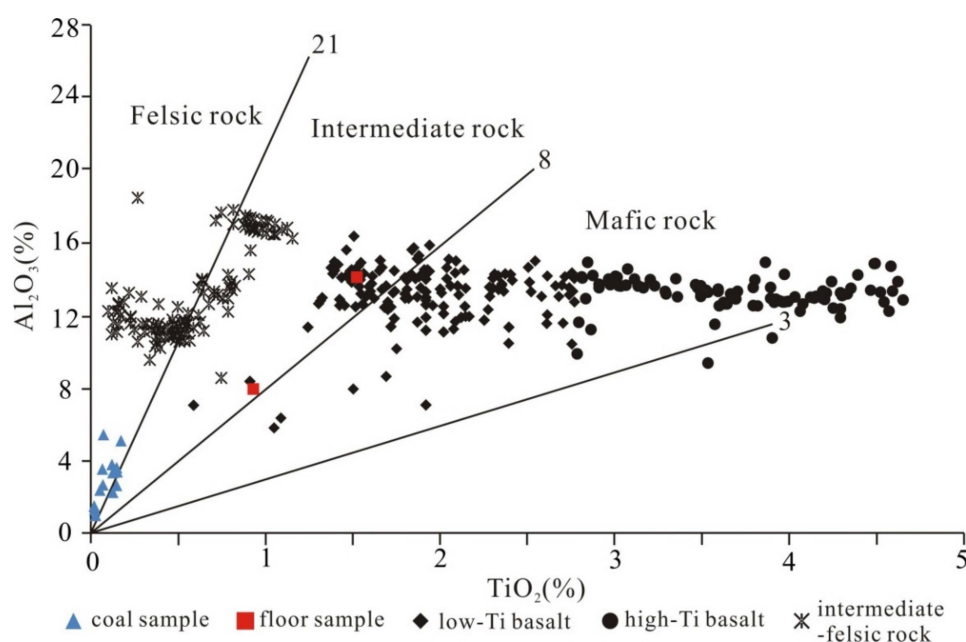

Figure 14. Plot of TiO_2 versus Al_2O_3 contents for coal and floor samples, in comparison to the low Ti basalt and high-Ti basalt [8,9,34–36] as well as intermediate-felsic rock [10,32,33].

The felsic parent rocks for the C4 Coal are also confirmed by the negative Eu anomalies (Figure 13). Europium anomaly is generally inherited from igneous rocks [69] because Eu fractionation from Eu^{3+} to Eu^{2+} mostly exists in the magmatic process [70]. The positive and negative Eu anomaly in sedimentary rocks including coal is believed to result from the input of mafic and felsic materials, respectively [69,71,72]. The C4 coals show strongly negative Eu anomalies ranging from 0.42 to 0.73 (Figure 13A), indicating a contribution from felsic rocks. Furthermore, the comparison of the plot of UCC-normalized REY distributions shows that the C4 Coal is more similar to the Guxu coals (Figure 13C) that originated from the Emeishan felsic rocks [21], than it is to the Zhina coals (Figure 13D) that were derived from the Emeishan basalts [12], also suggesting a felsic derivation.

The felsic parent rocks are not in accordance with the prior studies showing that the terrigenous materials for the Late Permian coals were mostly derived from the Kangdian Upland Emeishan basalts in Guizhou Province [6,11,12]. However, He et al. [24,25] indicated that the Emeishan felsic rocks at the uppermost part of the Kangdian Upland might have been a parent rock for the lowermost Late Permian strata in Southwestern China because felsic rocks were first eroded and transported. Dai et al. [20,21]

also reported that the terrigenous materials for the lowermost Late Permian coal seams in the Songzao Coalfield and Guxu Coalfield, respectively, were most likely the Emeishan felsic rocks at the uppermost part of the Kangdian Upland. In this study, the C4 Coal is also located at the lowermost portion of the Late Permian strata (Figure 2). Thus, the location of the C4 Coal, combined with the negative Eu anomalies (Figure 13) and high Al_2O_3/TiO_2 values (Figure 14), appears to suggest that the Emeishan felsic rocks at the top of the Kangdian Upland might have supplied detrital materials when the C4 Coal was being established. However, detrital materials from the subordinate uplifted region such as the Qianbei Uplift and Wenshui Highland may also have been introduced into the C4 Coal according to the following reasons:

(1) The Qianbei Uplift and Wenshui Highland to the south of the sampling site (Figure 1C) are subordinate exposure and erosion areas that might have served as sediment-source regions during the deposition of the lowermost Late Permian Wujiaping Formation strata in the Tongzi Coalfield [4,22]. However, the two subordinate source regions were submerged when the upper part of the Wujiaping Formation was being deposited due to extensive marine transgression [7,30].

(2) The Qianbei Uplift and Wenshui Highland consist mainly of the claystone derived from the Emeishan basaltic rocks or Maokou Formation limestones [6]. The claystone contains very low quartz amounts [20], due to silicon being easily dissolved and removed during weathering and leaching [73]. If the Qianbei Uplift and/or Wenshui Highland could have been the sediment-source region, a low quartz amount would be expected in the C4 coals, which is consistent with the present study (Figure 3).

(3) The SiO_2/Al_2O_3 ratio (0.66 on average) in the C4 Coal is apparently lower than the theoretical ratio for kaolinite (Figure 5), which is ascribed to the occurrence of Al-oxyhydroxide minerals (Figures 7B and 10D). Al-oxyhydroxide minerals are commonly considered to be derived from the weathering crust of sediment-source region [3,74–77]. The China Coal Geology Bureau [6] also reported the presence of Al-oxyhydroxide minerals in the claystone in the Qianbei Upland. Thus, the presence of Al-oxyhydroxide minerals in the C4 Coal most likely indicates a detrital input from the claystone at the top of the Maokou Formation in the Qianbei Upland and/or Wenshui Highland.

5.3. Origins of Minerals in the Coal and Floor Samples

5.3.1. Pyrite

It is well known that pyrite is commonly concentrated in the marine-influenced coals and its formation requires the supply of iron and SO_4^{2-} ions [47,51]. The abundant pyrite in the C4 Coal appears to indicate a sufficient Fe supply from the sediment source area. However, except for authigenic sulfides, carbonates, and sulfates, other minerals (e.g., kaolinite and tobelite) in amount are less than 8.0%, possibly indicating a low detrital material influx into the original peat swamp. This possible explanation is that as the peat swamp was being established, the claystone in the sediment source regions (e.g., Qianbei Upland) were progressively submerged by marine transgression, which results in the reduction of Fe^{3+} to Fe^{2+} in the claystone. Dissolved Fe^{2+}, rather than detrital Fe-bearing mineral phases, was subsequently introduced into the coal-forming environments by water.

5.3.2. Tobelite

Several reports have shown that tobelite is almost exclusively observed in high-rank coals, most notably in low volatile bituminous coals [21,76,78,79] and semi-anthracite-anthracite coals [48,80–83]. The forming temperature of tobelite in coals and associated non-coal rocks, although still controversial, is commonly assumed to be at least >200 °C [80–82,84,85]. However, Liu et al. [86] and Liang et al. [87] indicated that tobelite begins to form at a temperature of approximately 105 °C in the mudstone partings. Williams et al. [88,89] reported that the substitution of NH_4^+ with K^+ in mudstones occurs at a temperature of approximately 50–150 °C. In the present study, the C4 Coal has Ro values ranging from 1.59% to 1.95% (1.76% on average), appearing to indicate a forming temperature of approximately 150–170 °C [90]. Williams et al. [89] noted that the formation of tobelite depends mainly on temperature

and NH_4^+ concentration in pore fluids. A significant amount of nitrogen may be released at a temperature of 80–120 °C [88,89], which coincides with the highly volatile bituminous stage [90]. Thus, the bulk of tobelite in the C4 Coal was most likely generated at least shortly after the high-volatile bituminous stage.

As reported in the previously published literature, the formation of tobelite in coals and associated non-coal rocks has been ascribed to the alteration of illite by the isomorphic replacement of NH_4^+ with K^+ [83,88,89,91,92] due to a similarity in ionic radius and charge of NH_4^+ with K^+ [88,93]. Such a formation process of tobelite, however, is not the case for this study, because illite has not been identified in the C4 coals. Alternatively, tobelite is commonly interpreted to be formed from the interaction of kaolinite and nitrogen with rank advance [22,76,81,84–87]. The nitrogen involved in the formation of tobelite was probably generated from both bacterial decay and thermal decomposition of organic matter [88,89,94]; the released nitrogen may interact with H^+ to form NH4+, which is readily dissolved into pore fluids under reducing and moderately low pH conditions [89]. In this study, tobelite is found as cell filings or pore space infillings, intimately associated with kaolinite (Figures 7C and 8A–C), appearing to suggest that the tobelite may have originated from a kaolinite precursor by the interaction of kaolinite with NH_4^+ during coalification, the latter of which was derived from the thermally affected coalification of organic matter. Liang et al. [87] and Zheng et al. [93] indicated that kaolinite (1:1) and tobelite (2:1) have different layer types in the crystal structures, and thus the conversion of kaolinite into tobelite requires the involvement of NH_4^+ and Si^{4+} following the interaction: kaolinite+NH_4^++Si^{4+}→NH_4^+-illite. The SEM-EDS analysis of C4 Coal samples indicates that tobelite has a higher SiO_2/Al_2O_3 ratio (1.42 on average) than the theoretical ratio for kaolinite (1.18) and tobelite (1.35), possibly indicating the involvement of more Si into the tobelite formation.

It is reported that tobelite is formed in the NH_4^+-rich and K^+-poor environments due to K^+ being preferentially incorporated into tobelite [86,93]. In this study, the C4 coals contain very low K_2O amounts (0.08%): a trace amount of K_2O (0.32% on average) was only identified in the tobelite crystal by the SEM-EDS analysis, all of which indicate a K^+-depleted coal-forming environment. The released NH_4^+ cannot migrate and is progressively concentrated into coal seam due to low permeability when the coal was progressively compacted. Meanwhile, the coal seam can also act as a barrier that keeps outside K^+-bearing solution percolating into coal seam. Consequently, the elevated NH_4^+ concentration, along with low K^+ concentration, might have provided a favorable condition for the formation of tobelite.

Previous studies have suggested that NH_4^+ may be generally retained in clay minerals either by adsorption and ion exchange or by incorporation into the interlayer location of clay minerals (fixed-NH_4), the former of which is easily affected by local chemical variations and the latter of which is structurally bound in silicates and is not easily released [88,89,92]. Liu et al. [95,96] reported that the adsorbed NH_4^+ is easily leached out from clay minerals by water solution and a minor amount of fixed-NH_4 is also removed by NaCl or KCl solution. In this study, the concentration of exchangeable NH_4^+ reaches 0.076% of tobelite (Table 3), possibly indicating that a relevant amount of NH_4^+ is replaced with K^+ and/or Na^+ in the interlayer site of tobelite, which is consistent with the previous findings [95,96].

6. Conclusions

The lowermost Late Permian C4 Coal in the Tongzi Coalfield, which was developed on a substrate of claystone at the top of the Maokou Formation limestones, offers an opportunity to investigate the influence of claystone and the Emeishan felsic rocks on the mineralogical and geochemical characteristics. In contrast to other Late Permian coals in Guizhou Province, the terrigenous materials for the C4 Coal were most likely derived from two possible sediment-region sources, namely, the Emeishan felsic rocks at the uppermost part of the Kangdian Upland and the claystone from the subordinate Qianbei Upland and/or Weishui Highland, the former of which is evidenced by the high

Al$_2$O$_3$/TiO$_2$ ratio and strongly negative Eu anomaly and the latter of which is indicated by the low SiO$_2$/Al$_2$O$_3$ ratio and the presence of Al-oxyhydroxide minerals in the C4 Coal.

The formation of the C4 Coal was influenced by various degrees of marine influence, which could have resulted in the variations in amount of sulfides (e.g., pyrite) and elements with an affinity to Fe-sulfides. The tobelite identified in the C4 Coal (low-volatile bituminous) was probably generated by the interaction of pre-existing kaolinite with NH$_4^+$ at least shortly after the high-volatile bituminous stage under NH$_4^+$-rich and K$^+$-poor conditions.

References

1. Dai, S.; Ren, D.; Chou, C.-L.; Finkelman, R.B.; Seredin, V.V.; Zhou, Y. Geochemistry of trace elements in Chinese coals: A review of abundances, genetic types, impacts on human health, and industrial utilization. *Int. J. Coal Geol.* **2012**, *94*, 3–21. [CrossRef]

2. Finkelman, R.B.; Dai, S.; French, D. The importance of minerals in coal as the hosts of chemical elements: A review. *Int. J. Coal Geol.* **2019**, *212*. [CrossRef]

3. Ward, C.R. Analysis, origin and significance of mineral matter in coal: An updated review. *Int. J. Coal Geol.* **2016**, *165*, 1–27. [CrossRef]

4. Spiro, B.F.; Liu, J.; Dai, S.; Zeng, R.; Large, D.; French, D. Marine derived ^{87}Sr/^{86}Sr in coal, a new key to geochronology and palaeoenvironment: Elucidation of the India-Eurasia and China-Indochina collisions in Yunnan, China. *Int. J. Coal Geol.* **2019**, *215*, 103304. [CrossRef]

5. Dai, S.; Chekryzhov, I.Y.; Seredin, V.V.; Nechaev, V.P.; Graham, I.T.; Hower, J.C.; Ward, C.R.; Ren, D.; Wang, X. Metalliferous coal deposits in East Asia (Primorye of Russia and South China): A review of geodynamic controls and styles of mineralization. *Gondwana Res.* **2016**, *29*, 60–82. [CrossRef]

6. China Coal Geology Bureau. *Sedimentary Environments and Coal Accumulation of Late Permian Coal Formation in Western Guizhou, Southern Sichuan, and Eastern Yunnan, China*; Chongqing University Press: Chongqing, China, 1996; pp. 156–216. (In Chinese with English Abstract).

7. Shao, L.; Zhang, C.; Yan, Z.; Dong, D.; Gao, C.; Li, Y.; Xu, X.; Liang, W.; Yi, T.; Xu, X.; et al. Sequence-palaeogeography and coal accumulation of the Late Permian in South China. *J. Palaeogeogr.* **2016**, *18*, 905–919. (In Chinese with English Abstract).

8. Song, X.Y.; Zhou, M.F.; Tao, Y.; Xiao, J.F. Controls on the metal compositions of magmatic sulfide deposits in the Emeishan large igneous province, SW China. *Chem. Geol.* **2008**, *253*, 38–49. [CrossRef]

9. Xiao, L.; Xu, Y.G.; Mei, H.J.; Zheng, Y.F.; He, B.; Pirajno, F. Distinct mantle sources of low-Ti and high-Ti basalts from the western Emeishan large igneous province, SW China: Implications for plume–lithosphere interaction. *Earth Planet. Sci. Lett.* **2004**, *228*, 525–546. [CrossRef]

10. Xu, Y.G.; Chung, S.L.; Shao, H.; He, B. Silicic magmas from the Emeishan large igneous province, Southwest China: Petrogenesis and their link with the end-Guadalupian biological crisis. *Lithos* **2010**, *119*, 47–60. [CrossRef]

11. Li, B.; Zhuang, X.; Li, J.; Querol, X.; Font, O.; Moreno, N. Geological controls on mineralogy and geochemistry of the Late Permian coals in the Liulong Mine of the Liuzhi Coalfield, Guizhou Province, Southwest China. *Int. J. Coal Geol.* **2016**, *154*, 1–15. [CrossRef]

12.	Li, B.; Zhuang, X.; Li, J.; Querol, X.; Font, O.; Moreno, N. Enrichment and distribution of elements in the Late Permian coals from the Zhina Coalfield, Guizhou Province, Southwest China. *Int. J. Coal Geol.* **2017**, *171*, 111–129. [CrossRef]

13.	Zhuang, X.; Querol, X.; Zeng, R.; Xu, W.; Alastuey, A.; López-Soler, A.; Plana, F. Mineralogy and geochemistry of coal from the Liupanshui mining district, Guizhou, south China. *Int. J. Coal Geol.* **2000**, *45*, 21–37. [CrossRef]

14.	Dai, S.; Ren, D.; Hou, X.; Shao, L. Geochemical and mineralogical anomalies of the late Permian coal in the Zhijin Coalfield of Southwest China and their volcanic origin. *Int. J. Coal Geol.* **2003**, *55*, 117–138. [CrossRef]

15.	Dai, S.; Li, D.; Ren, D.; Tang, Y.; Shao, L.; Shi, Z. Geochemistry of the late Permian No. 30 Coal Seam, Zhijin Coalfield of Southwest China: Influence of the siliceous low-temperature hydrothermal fluid. *Appl. Geochem.* **2004**, *19*, 1315–1330. [CrossRef]

16.	Dai, S.; Ren, D.; Tang, Y.; Yue, M.; Hao, L. Concentration and distribution of elements in Late Permian coals from western Guizhou Province, China. *Int. J. Coal Geol.* **2005**, *61*, 119–137. [CrossRef]

17.	Dai, S.; Chou, C.-L.; Yue, M.; Luo, K.; Ren, D. Mineralogy and geochemistry of a Late Permian coal in the Dafang Coalfield, Guizhou, China: Influence from siliceous and iron-rich calcic hydrothermal fluids. *Int. J. Coal Geol.* **2005**, *61*, 241–258. [CrossRef]

18.	Zhang, J.; Ren, D.; Zhu, Y.; Chou, C.-L.; Zeng, R.; Zheng, B. Mineral matter and potentially hazardous trace elements in coals from Qianxi Fault Depression Area in southwestern Guizhou, China. *Int. J. Coal Geol.* **2004**, *57*, 49–61. [CrossRef]

19.	Zhuang, X.; Su, S.; Xiao, M.; Li, J.; Alastuey, A.; Querol, X. Mineralogy and geochemistry of the Late Permian coals in the Huayingshan coal-bearing area, Sichuan Province, China. *Int. J. Coal Geol.* **2012**, *94*, 271–282. [CrossRef]

20.	Dai, S.; Wang, X.; Chen, W.; Li, D.; Chou, C.-L.; Zhou, Y.; Zhu, C.; Li, H.; Zhu, X.; Xing, Y.; et al. A high-pyrite semianthracite of Late Permian age in the Songzao Coalfield, southwestern China: Mineralogical and geochemical relations with underlying mafic tuffs. *Int. J. Coal Geol.* **2010**, *83*, 430–445. [CrossRef]

21.	Dai, S.; Liu, J.; Ward, C.R.; Hower, J.C.; French, D.; Jia, S.; Hood, M.M.; Garrison, T.M. Mineralogical and geochemical compositions of Late Permian coals and host rocks from the Guxu Coalfield, Sichuan Province, China, with emphasis on enrichment of rare metals. *Int. J. Coal Geol.* **2016**, *166*, 71–95. [CrossRef]

22.	Dai, S.; Xie, P.; Jia, S.; Ward, C.R.; Hower, J.C.; Yan, X.; French, D. Enrichment of U-Re-V-Cr-Se and rare earth elements in the late Permian coals of the Moxinpo Coalfield, Chongqing, China: Genetic implications from geochemical and mineralogical data. *Ore Geol. Rev.* **2017**, *80*, 1–17. [CrossRef]

23.	Liu, J.; Song, H.; Dai, S.; Nechaev, V.P.; Graham, I.T.; French, D.; Nechaeva, E.V. Mineralization of REE-Y-Nb-Ta-Zr-Hf in Wuchiapingian coals from the Liupanshui Coalfield, Guizhou, southwestern China: Geochemical evidence for terrigenous input. *Ore Geol. Rev.* **2019**, *115*, 103190. [CrossRef]

24.	He, B.; Xu, Y.G.; Huang, X.L.; Luo, Z.Y.; Shi, Y.R.; Yang, Q.J.; Yu, S.Y. Age and duration of the Emeishan flood volcanism, SW China: Geochemistry and SHRIMP zircon U–Pb dating of silicic ignimbrites, post-volcanic Xuanwei Formation and clay tuff at the Chaotian section. *Earth Planet. Sci. Lett.* **2007**, *255*, 306–323. [CrossRef]

25.	He, B.; Xu, Y.G.; Zhong, Y.T.; Guan, J.P. The Guadalupian–Lopingian boundary mudstones at Chaotian (SW China) are clastic rocks rather than acidic tuffs: Implication for a temporal coincidence between the end-Guadalupian mass extinction and the Emeishan volcanism. *Lithos* **2010**, *119*, 10–19. [CrossRef]

26.	He, B.; Xu, Y.G.; Chung, S.L.; Xiao, L.; Wang, Y. Sedimentary evidence for a rapid, kilometer-scale crustal doming prior to the eruption of the Emeishan flood basalts. *Earth Planet. Sci. Lett.* **2003**, *213*, 391–405. [CrossRef]

27.	Editing Committee of Stratigraphy (ECS). *Permian in China*; Geological Publishing House: Beijing, China, 2000. (In Chinese with English Abstract).

28.	Xu, Y.G.; He, B.; Chung, S.L.; Menzies, M.A.; Frey, F.A. Geologic, geochemical, and geophysical consequences of plume involvement in the Emeishan flood-basalt province. *Geology* **2004**, *32*, 917–920. [CrossRef]

29.	Yang, R.; Bao, M.; Liao, L.; Wang, W.; Wei, H.; Wang, Q. Ancient weathering crust and its mineralization near the Middle-Upper Permian boundary in western Guizhou Province, China. *Acta Miner. Sin.* **2007**, *27*, 41–48. (In Chinese with English Abstract).

30. Gao, C. Sequence-Palaeogeography and Coal-Accumulation of Late Permian in Chuan-Yu-Dian-Qian, China. Ph.D. Thesis, China University of Mining & Technology, Bejing, China, 2015; 172p. (In Chinese with English Abstract).

31. Chung, S.L.; Jahn, B.M. Plume-lithosphere interaction in generation of the Emeishan flood basalts at the Permian-Triassic boundary. *Geology* **1995**, *23*, 889–892. [CrossRef]

32. Shellnutt, J.G.; Zhou, M.F. Permian peralkaline, peraluminous and metaluminous A-type granites in the Panxi district, SW China: Their relationship to the Emeishan mantle plume. *Chem. Geol.* **2007**, *243*, 286–316. [CrossRef]

33. Shellnutt, J.G.; Jahn, B.M. Formation of the Late Permian Panzhihua plutonic-hypabyssal-volcanic igneous complex: Implications for the genesis of Fe–Ti oxide deposits and A-type granites of SW China. *Earth Planet. Sci. Lett.* **2010**, *289*, 509–519. [CrossRef]

34. Song, X.Y.; Zhou, M.F.; Keays, R.R.; Cao, Z.M.; Sun, M.; Qi, L. Geochemistry of the Emeishan flood basalts at Yangliuping, Sichuan, SW China: Implications for sulfide segregation. *Contrib. Miner. Petrol.* **2006**, *152*, 53–74. [CrossRef]

35. Xiao, L.; Xu, Y.G.; Chung, S.L.; He, B.; Mei, H. Chemostratigraphic correlation of Upper Permian lavas from Yunnan Province, China: Extent of the Emeishan large igneous province. *Int. Geol. Rev.* **2003**, *45*, 753–766. [CrossRef]

36. Xu, Y.; Chung, S.L.; Jahn, B.M.; Wu, G. Petrologic and geochemical constraints on the petrogenesis of Permian–Triassic Emeishan flood basalts in southwestern China. *Lithos* **2001**, *58*, 145–168. [CrossRef]

37. ASTM Standard D3173-11. *Test Method for Moisture in the Analysis Sample of Coal and Coke*; ASTM International: West Conshohocken, PA, USA, 2011.

38. ASTM Standard D3174-11. Annual Book of ASTM Standards. In *Test Method for Ash in the Analysis Sample of Coal and Coke*; ASTM International: West Conshohocken, PA, USA, 2011.

39. ASTM Standard D3175-11. *Test Method for Volatile Matter in the Analysis Sample of Coal and Coke*; ASTM International: West Conshohocken, PA, USA, 2011.

40. Li, B.; Zhuang, X.; Querol, X.; Moreno, N.; Córdoba, P.; Li, J.; Zhou, J.; Ma, X.; Liu, S.; Shangguan, Y. The mode of occurrence and origin of minerals in the Early Permian high-rank coals of the Jimunai depression, Xinjiang Uygur Autonomous Region, NW China. *Int. J. Coal Geol.* **2019**, *205*, 58–74. [CrossRef]

41. Chung, F.H. Quantitative interpretation of X-ray diffraction patterns of mixtures: I. Matrix flushing method for quantitative multicomponent analysis. *J. Appl. Crystalogr.* **1974**, *7*, 519–525. [CrossRef]

42. Querol, X.; Whateley, M.; Fernandez-Turiel, J.; Tuncali, E. Geological controls on the mineralogy and geochemistry of the Beypazari lignite, Central Anatolia, Turkey. *Int. J. Coal Geol.* **1997**, *33*, 255–271. [CrossRef]

43. GB/T 1574-2007 (National Standard of P.R. China). *Test Method for Analysis of Coal Ash*; Standards Press of China: Beijing, China, 2007. (In Chinese)

44. MT/T 850-2000 (National Standard of P.R. China). *Classification for Mositure of Coal*; Standards Press of China: Beijing, China, 2000. (In Chinese)

45. GB/T 15224.1-2010 (National Standard of P.R. China). *Classification for Quality of Coal*; Standards Press of China: Beijing, China, 2010. Part 1: Ash Yield. (In Chinese)

46. ASTM Standard D388-12. *Standard Classification of Coals by Rank*; ASTM International: West Conshohocken, PA, USA, 2012; Reapproved 2007.

47. Chou, C.-L. Sulfur in coals: A review of geochemistry and origins. *Int. J. Coal Geol.* **2012**, *100*, 1–13. [CrossRef]

48. Zhao, L.; Ward, C.R.; French, D.; Graham, I.T.; Dai, S.; Yang, C.; Xie, P.; Zhang, S. Origin of a kaolinite-NH_4-illite-pyrophyllite-chlorite assemblage in a marine-influenced anthracite and associated strata from the Jincheng Coalfield, Qinshui Basin, Northern China. *Int. J. Coal Geol.* **2018**, *185*, 61–78. [CrossRef]

49. Wang, X.; Dai, S.; Chou, C.-L.; Zhang, M.; Wang, J.; Song, X.; Wang, W.; Jiang, Y.; Zhou, Y.; Ren, D. Mineralogy and geochemistry of Late Permian coals fromthe Taoshuping Mine, Yunnan Province, China: Evidences for the sources ofminerals. *Int. J. Coal Geol.* **2012**, *96*, 49–59. [CrossRef]

50. Rao, C.P.; Gluskoter, H.J. *Occurrence and Distribution of Minerals in Illinois Coals*; Circular 476; Illinois State Geological Survey: Urbana, IL, USA, 1973; 56p.

51. Ward, C.R. Minerals in bituminous coals of the Sydney Basin (Australia) and the Illinois Basin (USA). *Int. J. Coal Geol.* **1989**, *13*, 455–479. [CrossRef]

52. Ketris, M.P.; Yudovich, Y.E. Estimations of Clarkes for carbonaceous biolithes: World average for trace element contents in black shales and coals. *Int. J. Coal Geol.* **2009**, *78*, 135–148. [CrossRef]

53. Dai, S.; Seredin, V.V.; Ward, C.R.; Hower, J.C.; Xing, Y.; Zhang, W.; Song, W.; Wang, P. Enrichment of U–Se–Mo–Re–V in coals preserved within marine carbonate successions: Geochemical and mineralogical data from the Late Permian Guiding Coalfield, Guizhou, China. *Mineralium Deposita* **2015**, *50*, 159–186. [CrossRef]

54. Seredin, V.V.; Dai, S. Coal deposits as a potential alternative source for lanthanides and yttrium. *Int. J. Coal Geol.* **2012**, *94*, 67–93. [CrossRef]

55. Taylor, S.R.; McLennan, S.M. *The Continental Crust: Its Composition and Evolution*; Blackwell: Oxford, UK, 1985; 312p.

56. Dai, S.; Zhang, W.; Ward, C.R.; Seredin, V.V.; Hower, J.C.; Li, X.; Song, W.; Wang, X.; Kang, H.; Zheng, L.; et al. Mineralogical and geochemical anomalies of late Permian coals from the Fusui Coalfield, Guangxi Province, southern China: Influences of terrigenous materials and hydrothermal fluids. *Int. J. Coal Geol.* **2013**, *105*, 60–84. [CrossRef]

57. Murray, R.W.; Buchholtz ten Brink, M.R.; Jones, D.L.; Gerlach, D.C.; Russ III, G.P. Rare earth elements as indicators of different marine depositional environments in chert and shale. *Geology* **1990**, *18*, 268–271. [CrossRef]

58. Bullock, L.A.; Parnell, J.; Perez, M.; Armstrong, J.G.; Feldmann, J.; Boyce, A.J. High selenium in the Carboniferous Coal Measures of Northumberland, North East England. *Int. J. Coal Geol.* **2018**, *195*, 61–74. [CrossRef]

59. Çelik, Y.; Karayiğit, A.İ.; Querol, X.; Oskay, R.G.; Mastalerz, M.; Özer, M.S.K. Coal characteristics, palynology, and palaeoenvironmental interpretation of the Yeniköy coal of Late Oligocene age in the Thrace Basin (NW Turkey). *Int. J. Coal Geol.* **2017**, *181*, 103–123. [CrossRef]

60. Marynowski, L.; Pisarzowska, A.; Derkowski, A.; Rakociński, M.; Szaniawski, R.; Środoń, J.; Cohen, A.S. Influence of palaeoweathering on trace metal concentrations and environmental proxies in black shales. *Palaeogeogr. Palaeoclimatol. Palaeoecol.* **2017**, *472*, 177–191. [CrossRef]

61. Dai, S.; Luo, Y.; Seredin, V.V.; Ward, C.R.; Hower, J.C.; Zhao, L.; Liu, S.; Tian, H.; Zou, J. Revisiting the late Permian coal fromthe Huayingshan, Sichuan, southwestern China: Enrichment and occurrence modes of minerals and trace elements. *Int. J. Coal Geol.* **2014**, *122*, 110–128. [CrossRef]

62. Zhou, Y.; Bohor, B.F.; Ren, Y. Trace element geochemistry of altered volcanic ash layers (tonsteins) in Late Permian coal-bearing formations of eastern Yunnan and western Guizhou Province, China. *Int. J. Coal Geol.* **2000**, *44*, 305–324. [CrossRef]

63. Hayashi, K.I.; Fujisawa, H.; Holland, H.D.; Ohmoto, H. Geochemistry of 1.9 Ga sedimentary rocks from northeastern Labrador, Canada. *Geochim. Cosmochim. Acta* **1997**, *61*, 4115–4137. [CrossRef]

64. Young, G.M.; Nesbitt, H.W. Processes controlling the distribution of Ti and Al in weathering profiles, siliciclastic sediments and sedimentary rocks. *J. Sediment. Res.* **1998**, *68*, 448–455. [CrossRef]

65. Dai, S.; Li, T.; Seredin, V.V.; Ward, C.R.; Hower, J.C.; Zhou, Y.; Zhang, M.; Song, X.; Song, W. Origin of minerals and elements in the Late Permian coals, tonsteins, and host rocks of the Xinde Mine, Xuanwei, eastern Yunnan, China. *Int. J. Coal Geol.* **2014**, *121*, 53–78. [CrossRef]

66. Dai, S.; Yang, J.; Ward, C.R.; Hower, J.C.; Liu, H.; Garrison, T.M.; O'Keefe, J.M. Geochemical and mineralogical evidence for a coal-hosted uranium deposit in the Yili Basin, Xinjiang, northwestern China. *Ore Geol. Rev.* **2015**, *70*, 1–30. [CrossRef]

67. Dai, S.; Guo, W.; Nechaev, V.P.; French, D.; Ward, C.R.; Spiro, B.F.; Finkelman, R.B. Modes of occurrence and origin of mineral matter in the Palaeogene coal (No. 19-2) from the Hunchun Coalfield, Jilin Province, China. *Int. J. Coal Geol.* **2018**, *189*, 94–110. [CrossRef]

68. Hower, J.C.; Eble, C.F.; Dai, S.; Belkin, H.E. Distribution of rare earth elements in eastern Kentucky coals: Indicators of multiple modes of enrichment. *Int. J. Coal Geol.* **2016**, *160*, 73–81. [CrossRef]

69. Dai, S.; Graham, I.T.; Ward, C.R. A review of anomalous rare earth elements and yttrium in coal. *Int. J. Coal Geol.* **2016**, *159*, 82–95. [CrossRef]

70. Rard, J.A. Chemistry and thermodynamics of europium and some if its simpler inorganic compounds and aqueous species. *Chem. Rev.* **1985**, *85*, 555–582. [CrossRef]

71.　Cullers, R.L.; Chaudhuri, S.; Arnold, B.; Lee, M.; Wolf, C.W., Jr. Rare earth distributions in clay minerals and in the clay-sized fraction of the Lower Permian Havensville and Eskridge shales of Kansas and Oklahoma. *Geochim. Cosmochim. Acta* **1975**, *39*, 1691–1703. [CrossRef]

72.　Cullers, R.L. Implications of elemental concentrations for provenance, redox conditions, and metamorphic studies of shales and limestones near Pueblo, CO, USA. *Chem. Geol.* **2002**, *191*, 305–327. [CrossRef]

73.　Nesbitt, H.W.; Wilson, R.E. Recent chemical weathering of basalts. *Am. J. Sci.* **1992**, *292*, 740–777. [CrossRef]

74.　Dai, S.; Ren, D.; Chou, C.L.; Li, S.; Jiang, Y. Mineralogy and geochemistry of the no. 6 coal (Pennsylvanian) in the Junger Coalfield, Ordos Basin, China. *Int. J. Coal Geol.* **2006**, *66*, 253–270. [CrossRef]

75.　Dai, S.; Li, D.; Chou, C.L.; Zhao, L.; Zhang, Y.; Ren, D.; Sun, Y. Mineralogy and geochemistry of boehmite-rich coals: New insights from the Haerwusu Surface Mine, Jungar Coalfield, Inner Mongolia, China. *Int. J. Coal Geol.* **2008**, *74*, 185–202. [CrossRef]

76.　Dai, S.; Zou, J.; Jiang, Y.; Ward, C.R.; Wang, X.; Li, T.; Xue, W.; Liu, S.; Tian, H.; Sun, X.; et al. Mineralogical and geochemical compositions of the Pennsylvanian coal in the Adaohai Mine, Daqingshan Coalfield, Inner Mongolia, China: Modes of occurrence and origin of diaspore, gorceixite, and ammonian illite. *Int. J. Coal Geol.* **2012**, *94*, 250–270. [CrossRef]

77.　Dai, S.; Jiang, Y.; Ward, C.R.; Gu, L.; Seredin, V.V.; Liu, H.; Zhou, D.; Wang, X.; Sun, Y.; Zou, J.; et al. Mineralogical and geochemical compositions of the coal in the Guanbanwusu Mine, Inner Mongolia, China: Further evidence for the existence of an Al (Ga and REE) ore deposit in the Jungar Coalfield. *Int. J. Coal Geol.* **2012**, *98*, 10–40. [CrossRef]

78.　Permana, A.K.; Ward, C.R.; Li, Z.; Gurba, L.W. Distribution and origin of minerals in high-rank coals of the South Walker Creek area, Bowen Basin, Australia. *Int. J. Coal Geol.* **2013**, *116*, 185–207. [CrossRef]

79.　Wang, X.; Dai, S.; Ren, D.; Yang, J. Mineralogy and geochemistry of Al-hydroxide/oxyhydroxide mineral-bearing coals of Late Paleozoic age from the Weibei coalfield, southeastern Ordos Basin, North China. *Appl. Geochem.* **2011**, *26*, 1086–1096. [CrossRef]

80.　Dai, S.; Ji, D.; Ward, C.R.; French, D.; Hower, J.C.; Yan, X.; Wei, Q. Mississippian anthracites in Guangxi Province, southern China: Petrological, mineralogical, and rare earth element evidence for high-temperature solutions. *Int. J. Coal Geol.* **2018**, *197*, 84–114. [CrossRef]

81.　Daniels, E.J.; Altaner, S.P. Clay mineral authigenesis in coal and shale from the Anthracite region, Pennsylvania. *Am. Mineral.* **1990**, *75*, 825–839.

82.　Daniels, E.J.; Aronson, J.L.; Altaner, S.P.; Clauer, N. Late Permian age of NH4- bearing illite in anthracite from eastern Pennsylvania: Temporal limits on coalification in the central Appalachians. *Geol. Soc. Am. Bull.* **1994**, *106*, 760–766. [CrossRef]

83.　Ward, C.R.; Christie, P.J. Clays and other minerals in coal seams of the Moura-Baralaba area, Bowen Basin, Australia. *Int. J. Coal Geol.* **1994**, *47*, 31–49. [CrossRef]

84.　Daniels, E.J.; Altaner, S.P. Inorganic nitrogen in anthracite from eastern Pennsylvania, USA. *Int. J. Coal Geol.* **1993**, *22*, 21–35. [CrossRef]

85.　Sucha, V.; Kraus, I.; Madejova, J. Ammonium illite from anchimetamorphic shales associated with anthracite in the Zemplinicum of the Western Carpathians. *Clay Miner.* **1994**, *29*, 369–377. [CrossRef]

86.　Liu, Q.; Zhang, P.; Ding, S.; Lin, X.; Zheng, N. Ammoniumillite in Permo-Carboniferous coal-bearing strata, North China. *Chin. Sci. Bull.* **1996**, *41*, 717–719. (In Chinese)

87.　Liang, S.; Liu, Q.; Yu, C.; Song, H. Ammonium-bearing illite in tonsteins of Permo- Carboniferous coal accumulation area of Northern China. *J. Hebei Inst. Archit. Sci. Technol.* **2005**, *22*, 59–65, (In Chinese with English Abstract).

88.　Williams, L.B.; Ferrell, R.E., Jr.; Chinn, E.W.; Sassen, R. Fixed-ammonium in clays associated with crude oils. *Appl. Geochem.* **1989**, *4*, 605–616. [CrossRef]

89.　Williams, L.B.; Wilcoxon, B.R.; Ferrell, R.E.; Sassen, R. Diagenesis of ammonium during hydrocarbon maturation and migration, Wilcox Group, Louisiana, USA. *Appl. Geochem.* **1992**, *7*, 123–134. [CrossRef]

90.　Boudou, J.P.; Schimmelmann, A.; Ader, M.; Mastalerz, M.; Sebilo, M.; Gengembre, L. Organic nitrogen chemistry during low-grade metamorphism. *Geochim. Cosmochim. Acta* **2008**, *72*, 1199–1221. [CrossRef]

91.　Juster, T.C.; Brown, P.E.; Bailey, S.W. NH_4-bearing illite in very low grade metamorphic rocks associated with coal, northeastern Pennsylvania. *Am. Mineral.* **1987**, *72*, 555–565.

92.　Williams, L.B.; Ferrell, R.E. Ammonium substitution in illite during maturation of organic matter. *Clays Clay Miner.* **1991**, *39*, 400–408. [CrossRef]

93. Zheng, Q.; Liu, Q.; Shi, S. Mineralogy and geochemistry of ammonian illite in intra-seam partings in Permo-Carboniferous coal of the Qinshui Coalfield, North China. *Int. J. Coal Geol.* **2016**, *153*, 1–11. [CrossRef]

94. Hao, G. Characteristics, origin and geological significance of ammonium illite in coal measures. Ph.D. Thesis, China University of Mining & Technology, Bejing, China, 2013; 120p. (In Chinese with English Abstract).

95. Liu, Q.; Liu, L.; Shen, S.; Ding, S.; Zhen, L.; Cheng, H. Leaching experiments on nitrogen release from ammonium illite gangue. *J. China Coal Soc.* **2009**, *34*, 1022–1026, (In Chinese with English Abstract).

96. Liu, Q.; Liu, L.; Ding, S. The water-solubility and exchangeability of NH_4^+ in ammonium illite. *Acta Mineral. Sin.* **2010**, *3*, 3. (In Chinese with English Abstract).